

LIVER FIBROSIS

Targeting epigenetically maladapted vascular niche alleviates liver fibrosis in nonalcoholic steatohepatitis

Hua Zhang^{1†}, Yongyuan Ma^{1†}, Xinying Cheng^{1†}, Dongbo Wu^{2†}, Xingming Huang^{1†}, Bin Chen³, Yafeng Ren¹, Wei Jiang², Xiaoqiang Tang¹, Ting Bai⁴, Yutian Chen¹, Yilin Zhao¹, Chunxue Zhang¹, Xia Xiao¹, Jing Liu¹, Yue Deng⁵, Tinghong Ye¹, Lu Chen¹, Han-Min Liu¹, Scott L. Friedman⁶, Liping Chen^{7*}, Bi-Sen Ding^{1,6,8*}, Zhongwei Cao^{1,6*}

Chronic hepatic diseases such as nonalcoholic steatohepatitis (NASH) suppress liver regeneration and lead to fibrosis and cirrhosis. Decoding the cellular and molecular network underlying this fibrotic maladaptation might aid in combatting NASH, a growing health challenge with no approved therapies. Here, we used multiomics analysis of human cirrhotic liver, a Western diet- and carbon tetrachloride (CCl₄)-induced minipig NASH model, and genetically modified mice to unravel the landscape of the vascular adaptome at the single-cell level, in which endothelial cells (ECs) and T_H17 cells jointly contribute to liver cirrhosis. We found that epigenetics-dependent hepatic vascular maladaptation enriches fibrogenic T_H17 cells to promote liver fibrosis in mice, minipigs, and human patients with cirrhosis. Further analysis of humans, minipigs, and mice suggested that cross-talk between histone deacetylase 2 (HDAC2) and DNA methyltransferase 1 (DNMT1) promoted liver EC maladaptation to promote production of angiocrine IGFBP7 and ADAMTS1 in extracellular vesicles, recruiting fibrogenic T_H17 cells to the liver. Pharmacological targeting of HDAC2 and DNMT1 alleviated fibrosis in a minipig NASH model. We conclude that epigenetically reprogrammed vascular adaptation contributes to liver fibrosis. Targeting of a vascular adaptation node might block maladaptive vascularization to promote liver regeneration in NASH.

INTRODUCTION

Nonalcoholic steatohepatitis (NASH), a rising cause of chronic disease paralleling a global increase in diabetes and metabolic syndrome (1–4), leads to fibrosis, cirrhosis, and liver failure. Resulting liver fibrosis and cirrhosis are a major health burden worldwide without effective antifibrotic treatments, which frequently lead to systemic complications and comorbidities (5–7). One obstacle in developing NASH therapy is the gap between the clinical need and complementary human and preclinical studies that systematically model the cellular and molecular networks underlying NASH pathogenesis.

The liver is composed of parenchymal (hepatocytes) and non-parenchymal cells (NPCs) such as stellate, vascular endothelial, and hematopoietic cells (8, 9). Persistent stress in NASH frequently causes aberrant cellular cross-talk and stimulates maladaptive repair and fibrosis (2, 10, 11). Activation of stellate cells is the key step in liver fibrogenesis (12, 13), but it remains to be defined how chronic stress in NASH mediates the cross-talk between other liver NPCs to contribute to this step. Among NPCs, vascular and hematopoietic cells belong to the circulatory system and can directly transmit systemic

stimuli such as metabolic stress (14–19). They can also jointly establish a microenvironment that interacts with parenchymal or mesenchymal cells as niche cells (20, 21). Although chronic injury sometimes leads to genomic instability in parenchymal cells (22–26), gene mutation is rarely detected in niche cells such as endothelial cells (ECs) lining the vasculature (27–31). Hence, there might be additional epigenetic regulation involved in the maladaptation of the endothelial niche function during fibrogenesis, including histone and DNA modifications.

Vascular ECs lining the blood vessel are a major component of liver NPCs (15, 16, 21, 32–34). The hepatic blood supply is distributed by the sinusoidal vasculature between the hepatic vein, artery, and portal vein (35, 36). The sinusoidal vasculature is lined with a layer of fenestrated ECs expressing CLEC4G (37, 38) and OIT3 (27), and large-vessel (macrovascular) ECs lining the artery and vein preferentially express CD34 (39). Hence, liver ECs at different anatomical locations exhibit specialized morphology and phenotypic markers having “sinusoidal-macro” vascular hierarchy and intraorgan taxonomy. During organ repair, vascular ECs also produce a plethora of mediators to regulate the communication between hematopoietic, mesenchymal, and parenchymal cells (28, 32, 40, 41). Aberrant alteration of sinusoidal ECs (SECs) such as capillarization has been associated with liver fibrogenesis (42–44). However, the functional contribution of specialized liver EC subsets to human liver cirrhosis or NASH pathology has not been systemically delineated in complementary clinical and preclinical models at the single-cell level.

In this study, we combined single-cell RNA sequencing (scRNA-seq) of human patients and a large-animal NASH model to reveal how maladaptation of sinusoidal-macro vascular hierarchy stimulates a profibrotic T helper 17 (T_H17) cell response (45) in NASH. We further investigated the efficacy of combinatorial targeting of HDAC2/DNMT1 in blocking vascular niche maladaptation and promoting liver repair in the NASH animal models. Furthermore, both *Igfbp7* knockout mice and mice transplanted with angiocrine extracellular

¹Key Laboratory of Birth Defects and Related Diseases of Women and Children of MOE, State Key Laboratory of Biotherapy, West China Second University Hospital, Sichuan University, Chengdu 610041, China. ²Center of Infectious Diseases, West China Hospital, Sichuan University, Chengdu 610041, China. ³Institutes for Systems Genetics, Frontiers Science Center for Disease-related Molecular Network, West China Hospital, Sichuan University, Chengdu 610041, China. ⁴Department of Cardiology, The First Affiliated Hospital, Xi'an Jiaotong University, Xi'an 710061, China. ⁵Peking University China-Japan Friendship School of Clinical Medicine, Beijing 100029, China. ⁶Fibrosis Research Program, Division of Pulmonary and Critical Care Medicine, Division of Liver Diseases, Icahn School of Medicine at Mount Sinai, New York, NY 10029, USA. ⁷Department of Biliary Surgery, West China Hospital, Sichuan University, Chengdu 610041, China. ⁸Division of Regenerative Medicine, Weill Cornell Medicine, New York, NY 10065, USA.

*Corresponding author. Email: dingbisen@scu.edu.cn, bsding@outlook.com (B.-S.D.); 47137417@qq.com (L.C.); zhongweicao@scu.edu.cn (Z.C.)

†These authors contributed equally to this work.

vesicles (EVs) lacking ADAMTS1 exhibited reduction of liver fibrosis in the NASH model. These results further suggest that the beneficial effect is owing to suppressing angiocrine IGFBP7 and ADAMTS1 that enrich the fibrogenic T_H17 cells.

RESULTS

scRNA-seq reveals vascular maladaptation and distortion of endothelial taxonomy in human cirrhotic liver

NPCs were isolated from fresh healthy and cirrhotic human livers (Fig. 1A and table S1). scRNA-seq was performed by 10x Genomics. Clustering 22,374 NPCs from two healthy and two cirrhotic livers revealed 25 populations (fig. S1, A and B). Seven cell lineages were defined by the expression of marker genes, including T cell, B cell, EC, macrophage (Mac), neutrophil (Neu), dendritic cell (DC), and EPCAM⁺ cell and cholangiocytes (EPCAM⁺) (Fig. 1, B and C). We found that ECs exhibited the highest number of differentiated genes in the tested cell types, except for EPCAM⁺ cells with minimal cell numbers (Fig. 1D). The proportion of ECs increased in cirrhotic livers compared with healthy livers (fig. S1C).

Our previous studies have shown that ECs form a vascular niche by releasing paracrine/angiocrine factors that regulate liver regeneration and fibrosis (20). Therefore, we delineated EC subpopulations in human livers. Clustering of human liver ECs identified 12 clusters (fig. S1D) annotated as SEC and macrovascular/large-vessel EC (MEC) by marker genes *CLEC4G*, *OIT3*, and *CD34* (Fig. 1E and fig. S1E). There were an increased number of MECs and a decreased amount of SECs, implying maladaptation from SEC to MEC in cirrhotic human livers (Fig. 1, E and F). To verify this distortion of vascular endothelial taxonomy, we also analyzed the data from human liver dataset GSE136103 (37), where we observed a similar increase in MEC number and decrease in SEC quantity in cirrhotic human livers (fig. S2). The expression of mesenchymal cell markers was low in total ECs and cirrhotic ECs, and there was a relatively low enrichment of “mesenchymal cell differentiation” in tested types of liver ECs (fig. S3, A to C). These data suggest that liver SECs might undergo vascular maladaptation in fibrotic livers (fig. S3D).

Epigenetic reprogramming of liver ECs promotes profibrotic sinusoidal-to-macro vascular maladaptation

We then set out to define the contribution of vascular maladaptation to human liver fibrosis and its underlying mechanism. Epigenetic regulation (histone modification and DNA methylation) has been shown to play an important role in liver fibrosis (46–48). However, the functional role of histone and DNA modification in different NPC lineages in human liver fibrosis/cirrhosis remains unclear. A liquid chip analysis of histones H3 and H4 modification showed that histone acetylation of NPCs but not parenchymal cells was specifically reduced in human cirrhotic livers compared with healthy livers (Fig. 1G), suggesting an epigenetic reprogramming of NPCs in human cirrhotic liver.

We further explored the epigenetic changes in different NPC subpopulations from healthy and cirrhotic human livers. Among the tested cell types, vascular ECs manifested the most changes in histone modification and DNA methylation-related genes (cirrhotic versus healthy) (Fig. 1H). These findings raise the possibility that epigenetic changes in ECs might contribute to liver fibrosis by stimulating maladaptation of vascular niche function. Histone acetylation is regulated by HDACs. Human fibrotic livers were divided

into different pathological grades, F0 to F4, with F4 being the most severe fibrosis stage. In all HDACs, HDAC2 expression progressively increased in the livers of patients from grades F2 to F4 (Fig. 1I, fig. S4A, and data from GSE84044) (49). Moreover, HDAC2 expression was up-regulated in the ECs of human cirrhotic livers compared with those of healthy human livers (Fig. 1J). Quantitative polymerase chain reaction (qPCR) showed that there was no difference in HDAC2 expression in CD45⁺ NPCs between healthy and cirrhotic groups (fig. S4B). By contrast, the HDAC2 expression was up-regulated in the ECs of cirrhotic liver (CD45⁻CD31⁺) compared with those of healthy humans (Fig. 1K).

DNA methylation is another epigenetic modification that often synergizes with histone modification (48, 50). DNMT1 was also found to be the most induced in the fibrotic livers of patients from F2 to F4 (Fig. 1L and data from GSE84044), and DNMT1 expression was preferentially enhanced in the ECs of human cirrhotic livers relative to that of human healthy livers (Fig. 1, M and N, and fig. S4B). In isolated CD45⁻CD34⁻CD31⁺ SECs of human cirrhotic livers, HDAC2 and DNMT1 expression was significantly up-regulated compared with that of healthy human livers ($P < 0.05$) (Fig. 1O). Knockdown of HDAC2 by shRNA (shHDAC2) in human umbilical vein ECs (HUVECs) up-regulated the expression of DNMT1 (fig. S4C). These data suggest that aberrant activation of HDAC2 and DNMT1 in liver ECs might lead to sinusoidal-to-macro vascular maladaptation, promoting liver fibrosis and cirrhosis (fig. S4D).

Sequential targeting of HDAC2 and DNMT1 mitigates fibrosis in a minipig NASH model

Minipigs have unique physiological features that can resemble human metabolic disorders. Hence, we generated a minipig NASH model with Western diet (WD) combined with repeated carbon tetrachloride (CCl₄) injection (51) to interrogate the contribution of vascular maladaptation to liver cirrhosis and involved mechanisms. To delineate the pathological contribution of endothelial HDAC2/DNMT1 in this minipig NASH model, minipigs were also treated with HDAC2 inhibitor (HDAC2i) and DNMT1 inhibitor (DNMT1i) (Fig. 2, A and B). We found that blood glucose, liver fibrosis responses, liver function parameters, and total cholesterol in serum were elevated in the cirrhotic group compared with controls and decreased by HDAC2i + DNMT1i combinatorial treatment (Fig. 2, C to E). Thus, abnormal induction of HDAC2 and DNMT1 in ECs contributes to liver fibrosis and compromised liver function in the minipig NASH model.

Next, we assessed the histopathology, collagen deposition, and lipid droplet deposition in the livers of control, cirrhotic, and treated minipigs (Fig. 2, F and G). Compared with a control group showing normal histological features, the livers of cirrhotic animals manifested a unique pseudolobular phenotype. WD + CCl₄ induced advanced cirrhosis, collagen deposition, and lipid accumulation in the cirrhotic minipig group. HDAC2i + DNMT1i combinatorial treatment improved histopathological phenotype, decreased liver cirrhosis, and alleviated collagen deposition and lipid accumulation. This treatment also enhanced mitosis of liver cells with hepatocyte features such as distinctly round nuclei and polygonal shape, as evidenced by Ki67 staining (fig. S5, A to C). We then isolated minipig CD45⁻CD34⁻CD31⁺ SECs, CD45⁻CD34⁺CD31⁺ MECs, and other CD45⁺ NPCs by flow cytometry. There was no significant difference in the expression of HDAC2 and DNMT1 in CD45⁺ NPCs between different groups. By contrast, the expression of HDAC2 and DNMT1 was up-regulated in cirrhotic liver SECs and MECs

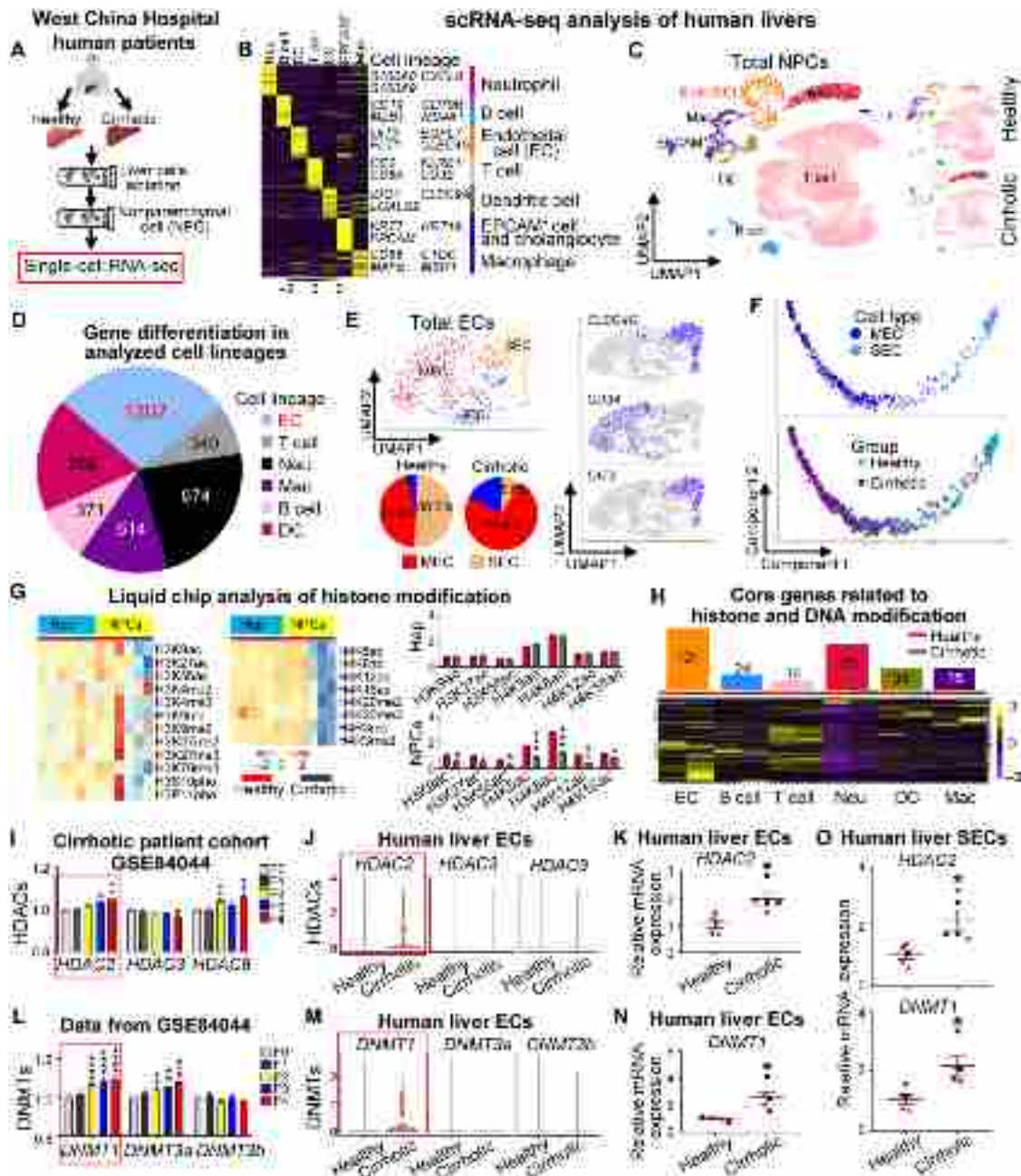


Fig. 1. scRNA-seq reveals a sinusoidal-to-macro vascular maladaptation in human cirrhotic liver, which is associated with HDAC2/DNMT1 induction in ECs. (A) Approach to generating a single-cell atlas of human liver NPCs. (B and C) Clustering analysis of scRNA-seq data from NPCs of two healthy and two cirrhotic livers. (B) Heatmap showing cluster marker genes and lineage annotation labeled (right). (C) Cell lineage inferred from expression of marker gene signatures (left) and annotation by group condition (right). Endo (EC), endothelial cell; DC, dendritic cell; Neu, neutrophil; Mac, macrophage; EPCAM⁺, EPCAM⁺ cell and cholangiocyte. (D) Pie chart showing quantification of gene differentiation in indicated cell lineages (cirrhotic versus healthy). (E) Clustering analysis of ECs from two healthy and two cirrhotic livers. Left: Cell lineage inferred from expression of marker gene signatures (top) and pie chart showing the proportion of EC subsets (bottom). Right: Selected marker gene expression. (F) Pseudotrajjectory analysis of different subsets of liver ECs from two healthy and two cirrhotic human livers. (G) Liquid chip analysis of histone modification in parenchymal hepatocytes and NPCs of healthy and cirrhotic human livers. Quantification of acetylation of different H3 and H4 modification sites is shown on right. Hep, hepatocytes. *n* = 3 per group. (H) Heatmap showing the expression of genes related to histone modification and DNA methylation in indicated cell lineages of two healthy and two cirrhotic human livers. Top: Number of differential genes related to histone modification and DNA methylation. (I) HDAC expression in human liver at different fibrosis stages. Expression of HDACs in the liver at F1 to F4 grades was quantified relative to that of healthy liver (F0). (J) Violin plot showing HDAC expression in two healthy and two cirrhotic human liver ECs. (K) qPCR of HDAC2 expression in liver ECs of healthy and cirrhotic humans. *n* = 5 per group. (L) Expression of DNMTs in human liver at different fibrosis stages. (M) Violin plot showing DNMT expression in liver ECs of two healthy and two cirrhotic humans. (N) qPCR of DNMT1 expression in liver ECs of healthy and cirrhotic humans. *n* = 5 per group. (O) qPCR of HDAC2 and DNMT1 expression in liver SECs of healthy and cirrhotic humans. *n* = 5 per group. Data were analyzed by unpaired two-tailed Student's *t* test with Shapiro-Wilk normality test (two-group comparisons) or one-way analysis of variance (ANOVA) followed by Tukey's post hoc test. Data are shown as means \pm SEM. *, cirrhotic versus healthy or F1 to F4 versus F0. **P* < 0.05; ***P* < 0.01; ****P* < 0.001; *****P* < 0.0001. Red, female; black, male.

Downloaded from https://www.science.org at Sichuan University on October 06, 2021

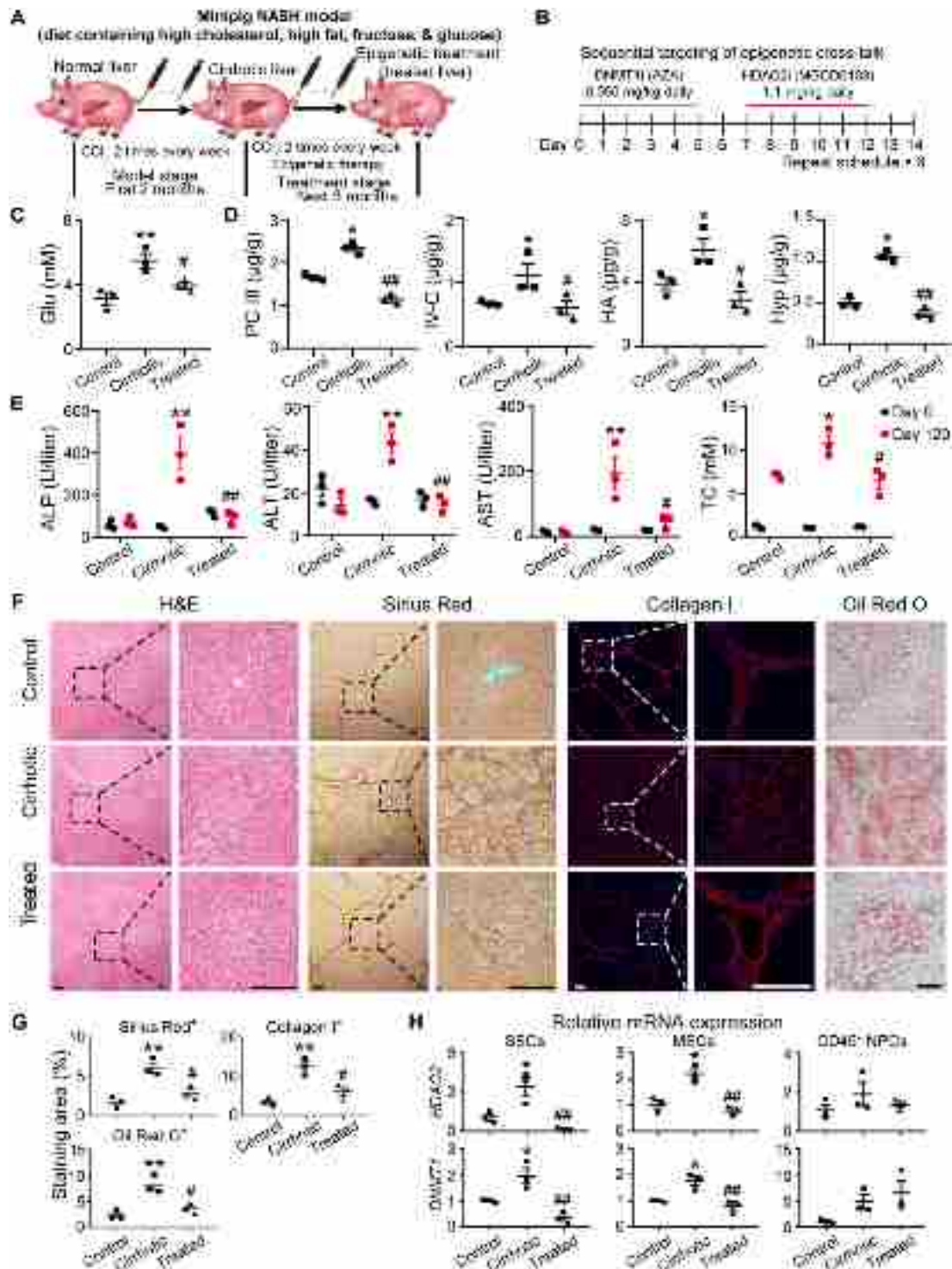


Fig. 2. Sequential targeting of HDAC2 and DNMT1 in liver ECs mitigates fibrosis in a minipig NASH model. (A) Minipig NASH model and treatment schema. (B) Approach to test the therapeutic effects of sequential inhibition of HDAC2 and DNMT1 in the minipig NASH model. (C to E) Blood glucose concentrations (C), fibrosis index (D), and serum liver function index (E) in control (healthy minipigs treated with vehicle), cirrhotic, and treated (HDAC2i + DNMT1i) minipigs. Glu, glucose; PC III, type III pro-collagen; IV-C, collagen IV; HA, hyaluronic acid; Hyp, hydroxyproline. $n = 3$ per group. (F and G) Liver histopathology was assessed by hematoxylin and eosin (H&E), Sirius Red, collagen I, and Oil Red O stainings from indicated minipig groups. Right: Magnified images of indicated dotted box areas. Quantifications of Sirius Red, Oil Red O, and collagen I staining are shown in (G). Scale bars, 200 μm . $n = 3$ per group. (H) qPCR results showing *HDAC2* and *DNMT1* transcription in liver SECs, MECs, and CD45⁺ NPCs of control, cirrhotic, and treated minipigs. $n = 3$ per group. For all statistical analyses, data were analyzed by one-way ANOVA followed by Tukey's post hoc test and are shown as means \pm SEM. *, cirrhotic versus control; #, treated versus cirrhotic. * $P < 0.05$; ** $P < 0.01$. # $P < 0.05$; ## $P < 0.01$.

compared with the control group, which was blocked by HDAC2i + DNMT1i treatment (Fig. 2H). The therapeutic effects of HDAC2i and DNMT1i in the minipig NASH model imply that aberrant HDAC2/ DNMT1 induction plays pathogenic role in NASH (fig. S5D).

Combinatorial epigenetic targeting normalizes maladapted liver endothelial taxonomy in a minipig NASH model

We next tested whether the aberrant induction of HDAC2/DNMT1 in minipig led to the sinusoidal-to-macro vascular maladaptation identified in human cirrhotic livers, with NPCs from the minipig NASH model defined at the single-cell level (Fig. 3A). We found the proportion (9.70% versus 5.90%) of ECs increased in minipig cirrhotic livers compared with healthy livers, which was reduced by HDAC2i + DNMT1i treatment (4.55% versus 9.70%) (Fig. 3, B to D, and fig. S6A). Vascular ECs in cirrhotic minipigs exhibited the highest degree of gene differentiation among the tested cell types, most of which was restored by HDAC2i + DNMT1i treatment (Fig. 3E). Gene Ontology (GO) analysis and pathway enrichment showed that there was significant change ($P < 0.05$) in gene expression in molecular function, biological process, and cellular component categories (fig. S6B), as well as in Kyoto Encyclopedia of Genes and Genomes (KEGG) pathways including T_H17 cell differentiation, nonalcoholic fatty liver disease (NAFLD), and chemokine, tumor necrosis factor, hypoxia-inducible factor 1 (HIF-1), mitogen-activated protein kinase, and phosphatidylinositol 3-kinase (PI3K)–Akt signaling (Fig. 3F). Moreover, 79 KEGG pathways were differentially expressed between cirrhotic and control groups, 53 of which were restored by HDAC2i + DNMT1i (Fig. 3F).

The influence of epigenetic changes on the ECs in the minipig NASH model led us to explore the linkage between HDAC2/DNMT1 activity and disruption of vascular endothelial taxonomy in liver fibrosis. The proportion of MECs was also increased, and SECs were reduced in minipig cirrhotic livers compared with control livers. HDAC2i + DNMT1i treatment reversed the distorted vascular hierarchy in treated minipig livers (Fig. 3, G and H, and fig. S7, A to C). In EC subsets, SECs manifested the highest number (1207) of differentially expressed genes between cirrhotic and control groups, 803 of which were restored by HDAC2i + DNMT1i (Fig. 3I). Pseudotrajectory analysis of liver EC subsets also suggested a sinusoidal-to-macro vascular maladaptation in minipig cirrhotic livers, which was normalized by HDAC2i + DNMT1i treatment (Fig. 3J). We also found that SECs manifested the most changes in histone modification and DNA methylation-related genes in cirrhotic minipigs, again restored by HDAC2i + DNMT1i treatment (fig. S7, D to F). Hence, our data from the minipig NASH model suggest that abnormal epigenetic alteration stimulates sinusoidal-to-macro vascular maladaptation and enhances fibrosis (fig. S7G).

Epigenetically maladapted SECs exhibit a reprogrammed paracrine/angiocrine landscape in human patients and a minipig NASH model

ECs modulate liver repair by supplying paracrine/angiocrine factors that interact with surrounding cells (20, 40, 52). To decipher the mechanism whereby epigenetically maladapted liver ECs promote fibrosis, we analyzed the differentially expressed angiocrine genes in the cirrhotic human and minipig ECs at the single-cell level (fig. S8A) and observed a reprogrammed angiocrine landscape associated with vascular maladaptation (Fig. 4, A to D). We found that *IGFBP7* and *ADAMTS1* expression were progressively elevated

in the fibrotic livers of patients from F2 to F4 grades (Fig. 4B). *IGFBP7* and *ADAMTS1* were specifically expressed in human and minipig ECs to the greatest extent among angiocrine genes (Fig. 4C and fig. S8, B and C). Moreover, *IGFBP7* and *ADAMTS1* were selectively up-regulated in human cirrhotic ECs compared with healthy ECs, and there was a significant increase in the mRNA and protein abundance of *IGFBP7* and *ADAMTS1* in cirrhotic SECs ($P < 0.05$) (Fig. 4, E and F). These results suggest an epigenetic reprogramming of the angiocrine landscape in maladapted human liver ECs, and that angiocrine *IGFBP7* and *ADAMTS1* might promote liver fibrosis and cirrhosis.

In the minipig NASH model, the mRNA abundance of *IGFBP7* and *ADAMTS1* were higher in cirrhotic SECs and MECs, but the protein abundance of *IGFBP7* and *ADAMTS1* were up-regulated only in cirrhotic SECs. Treatment of HDAC2i and DNMT1i blocked the increase of *IGFBP7* and *ADAMTS1* mRNA and protein in cirrhotic minipig SECs (Fig. 4, G to L, and fig. S8D). The assay for transposase-accessible chromatin using sequencing (ATAC-seq) (53) showed that chromatin accessibility in *IGFBP7* and *ADAMTS1* promoters was enhanced in cirrhotic ECs compared with control ECs and diminished by HDAC2i + DNMT1i (Fig. 4M). Hence, *IGFBP7* and *ADAMTS1* up-regulation might demarcate maladapted SECs from normal SECs in cirrhotic liver, and epigenetic targeting of the profibrotic *IGFBP7*⁺*ADAMTS1*⁺ maladapted EC subset might block liver fibrosis (fig. S8E).

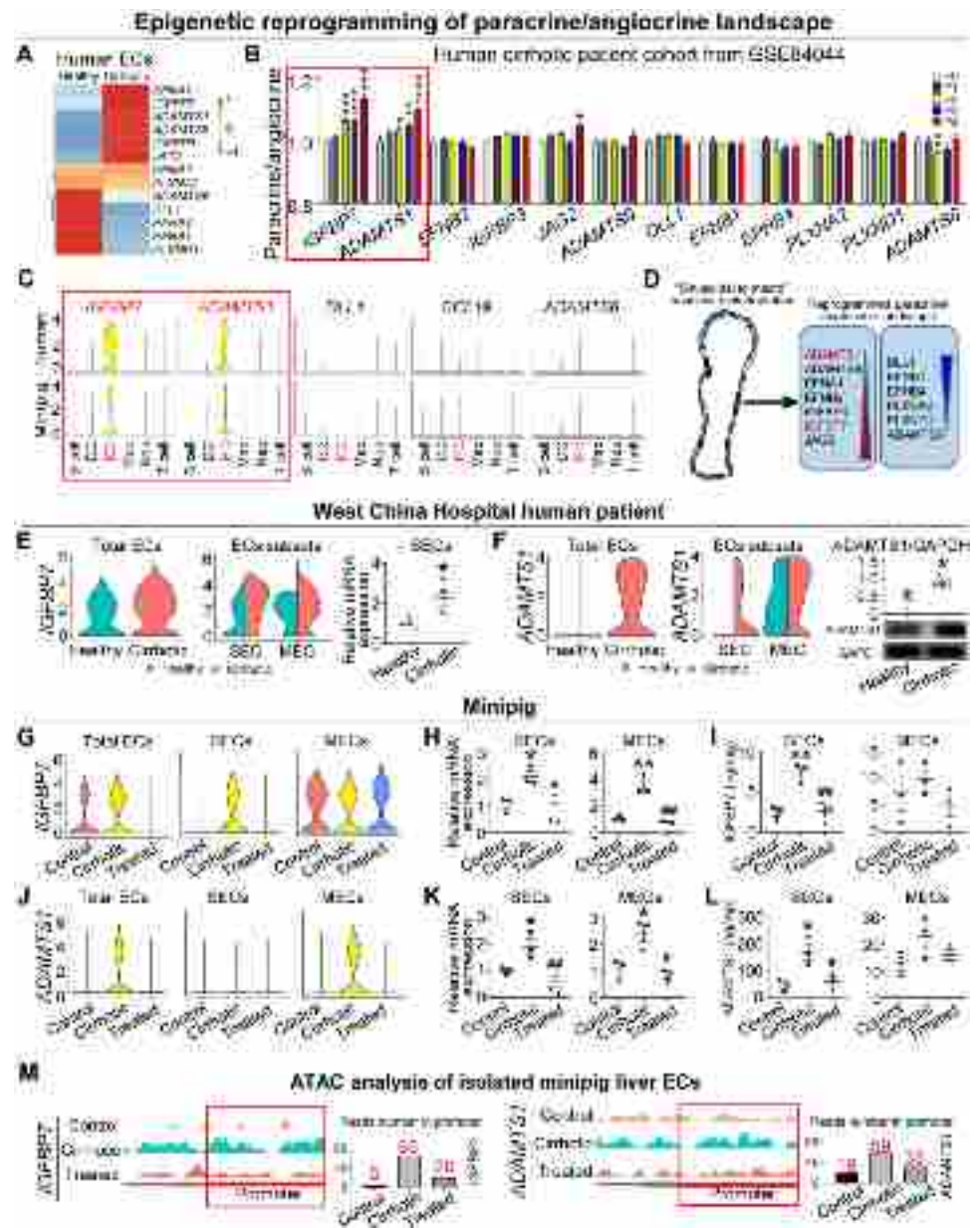
IGFBP7 and ADAMTS1 from maladapted SECs predict the progression and therapeutic outcome of liver fibrosis in humans and minipigs

To establish the clinical value of circulating *IGFBP7* and *ADAMTS1* in human liver fibrosis/cirrhosis or NASH, we assessed the concentrations of *IGFBP7* and *ADAMTS1* in human patient plasma (data file S1). Fibrotic/cirrhotic patients showed higher plasma concentrations of *IGFBP7*, *ADAMTS1*, alanine aminotransferase (ALT), and aspartate aminotransferase (AST) than those of healthy human samples (Fig. 5A). Because some fibrotic/cirrhotic patients can have normal plasma ALT or AST concentrations, there is a need to uncover sensitive biomarkers to diagnose liver fibrosis and cirrhosis in clinics (54). Therefore, we evaluated the value of plasma *IGFBP7* and *ADAMTS1* as clinical biomarkers. Fibrotic/cirrhotic patients were divided into two groups based on their plasma liver function index: those with normal or abnormal plasma ALT and AST concentrations (Fig. 5B). Of importance, plasma concentrations of *IGFBP7* and *ADAMTS1* in fibrotic/cirrhotic patients with normal ALT or AST were higher than those of healthy humans (Fig. 5C). The fibrotic/cirrhotic patient cohort included hepatitis B–related fibrosis/cirrhosis, NASH-related fibrosis/cirrhosis, autoimmune hepatitis–related fibrosis/cirrhosis, primary biliary fibrosis/cirrhosis, and cryptogenic fibrosis/cirrhosis. An increase in plasma *IGFBP7* and *ADAMTS1* abundance was observed in all these patients compared with healthy humans (Fig. 5D). Therefore, angiocrine *IGFBP7* and *ADAMTS1* associate with liver fibrosis/cirrhosis in the absence of hepatic dysfunction.

Next, we evaluated whether plasma *IGFBP7* and *ADAMTS1* associated with the severity of NASH or distinguished NASH from simple steatosis. Patients with NASH were divided into different groups according to liver fibrosis stages. Patients with early-stage NASH (F0 to F1) showed little increase in plasma ALT or AST concentration (Fig. 5E). By contrast, plasma *IGFBP7* and *ADAMTS1*

Fig. 4. Epigenetically maladapted liver ECs exhibit a reprogrammed paracrine/angiocrine landscape in human patients and minipigs.

(A) Heatmap showing representative endothelial paracrine/angiocrine genes differentially expressed by human cirrhotic liver ECs relative to ECs in healthy liver. $n = 2$ per group. (B) Paracrine/angiocrine gene expression in bulk human liver tissues at different fibrosis stages. (C) Violin plot showing the expression of representative paracrine/angiocrine genes of different NPC lineages in humans and minipigs. $P < 0.01$ for *IGFBP7* and *ADAMTS1*. (D) Schematic illustration of reprogrammed paracrine/angiocrine landscape associated with sinusoidal-to-macro vascular maladaptation. (E) *IGFBP7* expression in total ECs (left), different EC subsets (middle), and SECs (right) from healthy and cirrhotic human livers. $n = 2$ per group for scRNA-seq, $n = 5$ per group for qPCR. (F) *ADAMTS1* protein in total ECs (left), EC subsets (middle), and SECs (right) from healthy and cirrhotic human livers. Left: Violin plot showing *ADAMTS1* expression in total ECs. Middle: Violin plot showing *ADAMTS1* expression in different EC subsets. Right: Western blot showing *ADAMTS1* protein level in SECs. Top right: Quantification of protein expression. Bottom right: Representative blot image. scRNA-seq, $n = 2$ per group; Western blots, $n = 5$ per group. (G) *IGFBP7* mRNA in liver total ECs and EC subsets from one control, two cirrhotic, and two treated minipigs. (H and I) qPCR (H) and ELISA (I) results showing *IGFBP7* expression in liver SECs and MECs from control (healthy minipigs treated with vehicle), cirrhotic, and treated (HDAC2i + DNMT1i) minipigs. $n = 3$ per group. (J) *ADAMTS1* expression in liver total ECs and EC subsets from one control, two cirrhotic, and two treated minipigs. (K and L) qPCR (K) and ELISA (L) results showing *ADAMTS1* expression in liver SECs and MECs from control, cirrhotic, and treated minipigs. $n = 3$ per group. (M) ATAC-seq results showing reads mapped to *IGFBP7* and *ADAMTS1* promoters in liver ECs of indicated minipig groups. Unpaired two-tailed Student's t test with Welch's correction was applied in (E), unpaired two-tailed Student's t test was applied in (F), and one-way ANOVA followed by Tukey's post hoc test was used in comparisons between three groups. Data are shown as means \pm SEM. *, cirrhotic versus control (minipig) or healthy (human), or F1 to F4 versus F0; #, treated versus cirrhotic (minipig). * $P < 0.05$; ** $P < 0.01$; *** $P < 0.001$. # $P < 0.05$; ## $P < 0.01$. Red, female; black, male.



SECs depends on angiocrine IGFBP7 and ADAMTS1. Molecules packed in EVs might facilitate cellular communication in many biological processes (55, 56). Therefore, we analyzed if endothelial-produced IGFBP7 and ADAMTS1 are assembled in EVs and released into circulation. To this end, EVs were extracted from human and minipig plasma by ultracentrifugation (57) and characterized by electron microscope and immunoblot analysis (Fig. 5G). IGFBP7 and ADAMTS1 concentrations in minipig and human EVs were higher in the cirrhotic group than in the control group. In the minipig NASH model, elevated EV IGFBP7/ADAMTS1 concentrations in the cirrhotic group were reduced by HDAC2i + DNMT1i treatment (Fig. 5H). IGFBP7/ADAMTS1 concentrations in the EVs of fibrotic/cirrhotic human patients with normal ALT/AST or patients with NASH were also

increased compared with those of healthy humans (Fig. 5, I to J). Our data suggest that IGFBP7 and ADAMTS1 in EVs correlate with NASH progression (fig. S9).

IGFBP7⁺ADAMTS1⁺ maladapted SECs induce a profibrotic T_H17 response in cirrhotic patients and a minipig NASH model

Aberrantly activated ECs can form a maladaptive niche to promote fibrosis by interacting with adjacent cells. We sought to reveal the cellular communication mechanism whereby IGFBP7⁺ADAMTS1⁺ SECs enhance liver fibrosis. Receptor and ligand expression profiles in different NPC cell lineages were analyzed on the basis of the CellPhoneDB database (58). Cell interaction predictions suggested

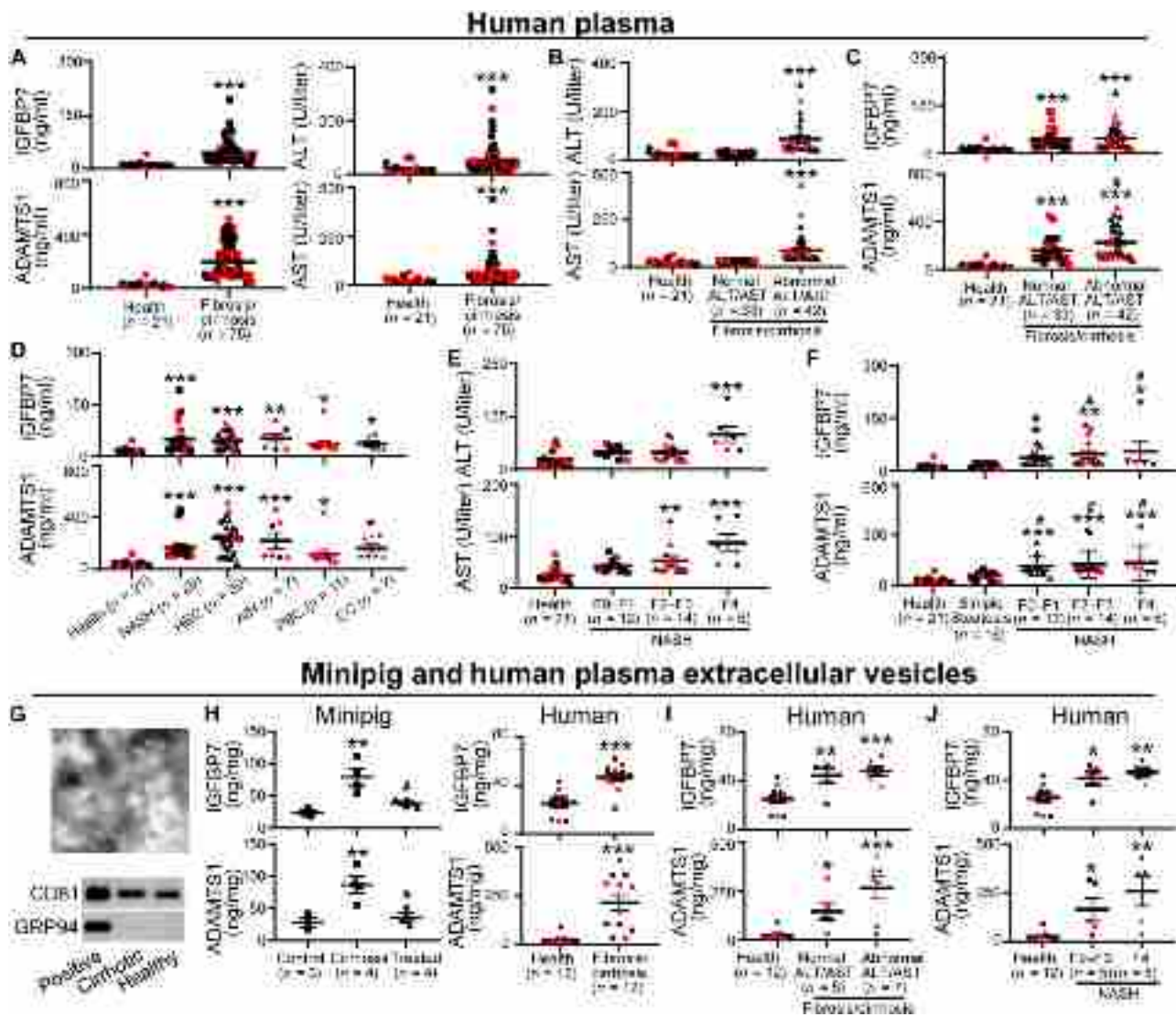


Fig. 5. Paracrine/angiocrine IGFBP7 and ADAMTS1 in EVs associate with fibrosis progression in human patients and a minipig NASH model. (A) Plasma concentrations of IGFBP7, ADAMTS1, ALT, and AST in healthy and fibrotic/cirrhosis patients. (B and C) Plasma concentrations of IGFBP7 and ADAMTS1 in fibrotic/cirrhosis patients with normal or abnormal liver function. (D) Plasma concentrations of IGFBP7 and ADAMTS1 in fibrotic/cirrhosis patients. NASH, NASH-related fibrosis/cirrhosis; HBC, hepatitis B-related fibrosis/cirrhosis; ALH, autoimmune hepatitis-related fibrosis/cirrhosis; PBC, primary biliary fibrosis/cirrhosis; CC, cryptogenic fibrosis/cirrhosis. (E) Plasma concentrations of ALT/AST in healthy individuals or patients with NASH with different pathological grades. (F) Plasma concentrations of IGFBP7 and ADAMTS1 in healthy, simple steatosis, and patients with NASH with different pathological grades. (G) Characterization of EVs purified from human plasma. Top: Electron microscopic analysis of purified EVs. Bottom: Western blot examining the EV marker CD81 and GRP94 as negative control. (H) Concentrations of IGFBP7/ADAMTS1 in the EVs purified from indicated minipig and human groups. (I and J) IGFBP7/ADAMTS1 concentrations in the EVs from fibrotic/cirrhosis patients with normal or abnormal liver function as indicated by ALT/AST (I) or patients with NASH with different fibrosis grades (J). Unpaired two-tailed Student's *t* test with Welch's correction was applied in (A), unpaired two-tailed Student's *t* test was applied in human IGFBP7 experiment in (H), Mann-Whitney nonparametric test without Shapiro-Wilk normality test was used in human ADAMTS1 experiment in (H), and one-way ANOVA followed by Tukey's post hoc test was used in comparison between more than two groups. Data are shown as means \pm SEM. *, fibrotic, cirrhotic, or NASH versus control (minipig) or healthy (human); #, NASH versus simple steatosis (human) or treated versus cirrhotic (minipig). **P* < 0.05; ***P* < 0.01; ****P* < 0.001. #*P* < 0.05. Red, female; black, male.

that maladapted ECs interact with T cells in both cirrhotic patients and NASH minipigs (Fig. 6A). Although most predicted interactions were found between human ECs and Macs, EC-Mac predicted interactions were lower in minipig NPCs. Because T cells were the most abundant liver NPC type in the analysis, we went on to analyze the interaction between ECs and T cells. Previous studies have shown the synergistic or complementary action between IGFBP7, ADAMTS1, and transforming growth factor- β 1 (TGF- β 1) (59, 60)

to recruit T_H17 cells, a $CD4^+$ T subset (61) involved in the progression of NASH and liver fibrosis (62, 63). Because Smad2 is an essential downstream factor for TGF- β 1-dependent generation of T_H17 cells (64, 65), we analyzed Smad2 phosphorylation in human liver $CD45^+$ NPCs. Smad2 phosphorylation was increased in cirrhotic human $CD45^+$ NPCs compared with healthy NPCs (Fig. 6B). We next analyzed the cell lineages in recruited human and minipig T cells. Clustering of human T cells from two cirrhotic and two healthy

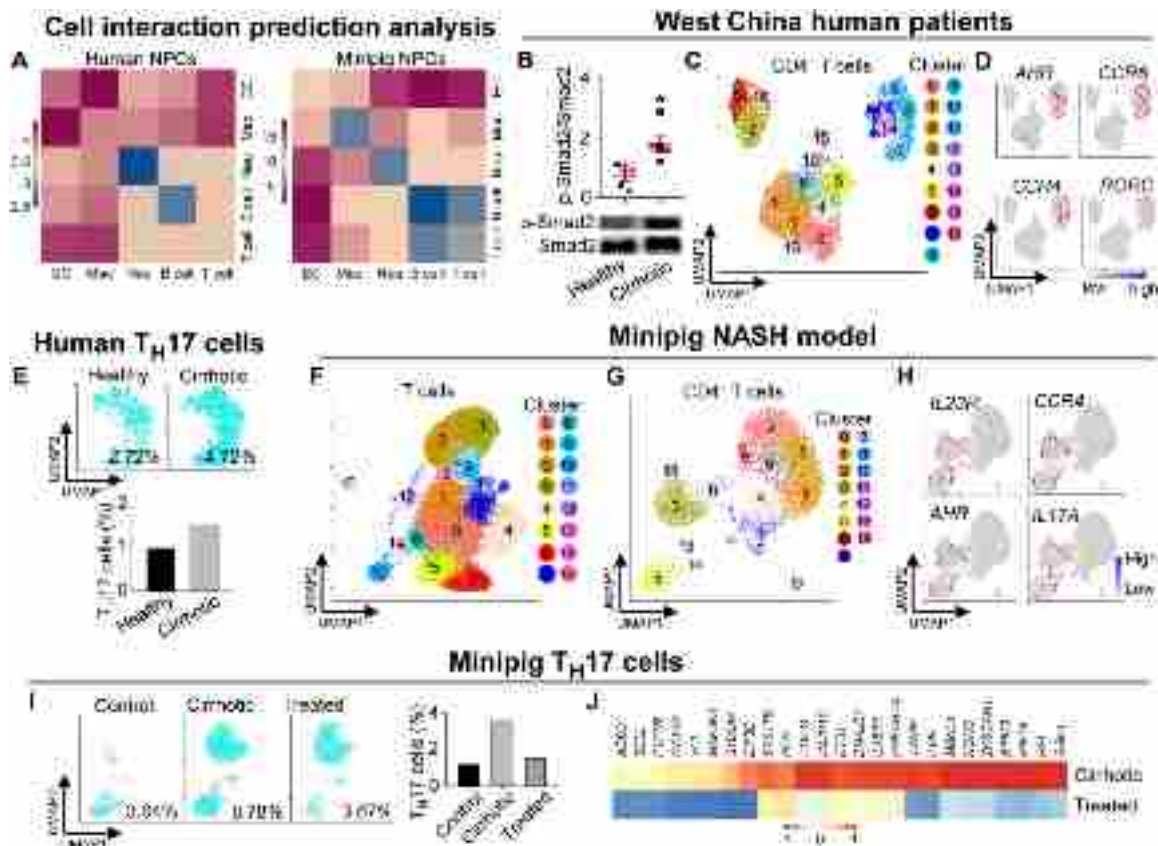


Fig. 6. A maladaptive endothelial niche enables a profibrotic T_H17 response in human patients and a minipig NASH model. (A) Cellular interaction prediction in different NPC cell lineages from scRNA-seq data from humans and minipigs. (B) Protein abundance of phosphorylated Smad2 in healthy and cirrhotic $CD45^+$ NPCs analyzed by Western blot. Data were analyzed by unpaired two-tailed Student's *t* test with Shapiro-Wilk normality test and are shown as means \pm SEM. *, cirrhotic versus healthy, $P < 0.05$. Red, female; black, male, $n = 5$ per group. (C) Clustering analysis of $CD4^+$ T cells from two healthy and two cirrhotic human livers. (D) Expression of T_H17^+ marker genes in T cell clusters of different human liver groups. (E) T_H17 cell proportion in the liver NPCs of different human groups quantified relative to that of healthy individuals. (F and G) Clustering analysis of T cells and $CD4^+$ T cells from one control, two cirrhotic, and two treated minipig livers. (H) Expression of T_H17^+ marker genes in $CD4^+$ T cell clusters of different minipig groups. (I) Characterization of T_H17 cells in NPCs of cirrhotic and treated minipig groups. Proportion of T_H17 cells was quantified relative to that of the control (healthy minipigs treated with vehicle) group. (J) Heatmap showing the differential expression of fibrosis-related genes in T_H17 cells of cirrhotic and treated minipig livers.

livers identified 20 clusters (fig. S10A) annotated as $CD4^+$ or $CD8^+$ T cells (fig. S10B). $CD4^+$ T cells were further clustered (Fig. 6C), and T_H17 cells were labeled by T_H17^+ marker genes (Fig. 6D). There were more T_H17 cells in the liver of cirrhotic patients compared with healthy liver (Fig. 6E). To verify our human patient results, we analyzed T_H17 cells using data from GSE136103 (fig. S10, C to I). In this dataset, there was a similar increase in T_H17 cell number in the cirrhotic human liver compared with healthy human liver. These data implicate the profibrotic role of T_H17 cells in human liver cirrhosis.

We next explored the cellular cross-talk between liver ECs and the T_H17 subset in the minipig NASH model. T_H17 cells were also more abundant in cirrhotic minipig livers compared with controls and were decreased in number by HDAC2i + DNMT1i treatment (Fig. 6, F to I, and fig. S10J). The expression of fibrosis-related genes was decreased in the T_H17 cells of treated minipigs compared with those of cirrhotic minipigs (Fig. 6J). Our data raise the hypothesis that epigenetically maladapted SECs might recruit and activate profibrotic T_H17 cells in human and minipig livers (fig. S10K).

Epigenetically maladapted SECs generate a profibrotic T_H17 response in a mouse NASH model

To establish the functional contribution of the HDAC2/DNMT1–IGFBP7/ADAMT1 axis in ECs to T_H17 cell activation and liver fibrosis, we generated an *Hdac2*^{iAEC} mouse in which *Hdac2* was selectively deleted in mouse ECs. Resulting *Hdac2*^{iAEC} mice were tested in a NASH model induced by WD and CCl₄ injury (Fig. 7A) (51). The therapeutic effect of combinatorial targeting of HDAC2/DNMT1 was tested by treating *Hdac2*^{iAEC} mice with DNMT1i azacitidine (AZA) (*Hdac2*^{iAEC} + AZA group). Liver fibrosis, inflammation, collagen deposition, and index of liver fibrosis and liver function were lower in *Hdac2*^{iAEC} mice treated with AZA than in control injured mice (Fig. 7B and fig. S11A). To further investigate the cross-talk between endothelial HDAC2 and DNMT1 in mouse liver SECs, we purified liver $CD45^+CD34^+CD31^+$ SECs by Dynabeads from control, *Hdac2*^{iAEC}, and *Hdac2*^{iAEC} + AZA mice. Western blotting showed that knockout of *Hdac2* in mouse liver SECs up-regulated the expression of DNMT1 in SECs (Fig. 7C). In this mouse NASH model, CD34 was expressed in some SECs, and targeting of endothelial

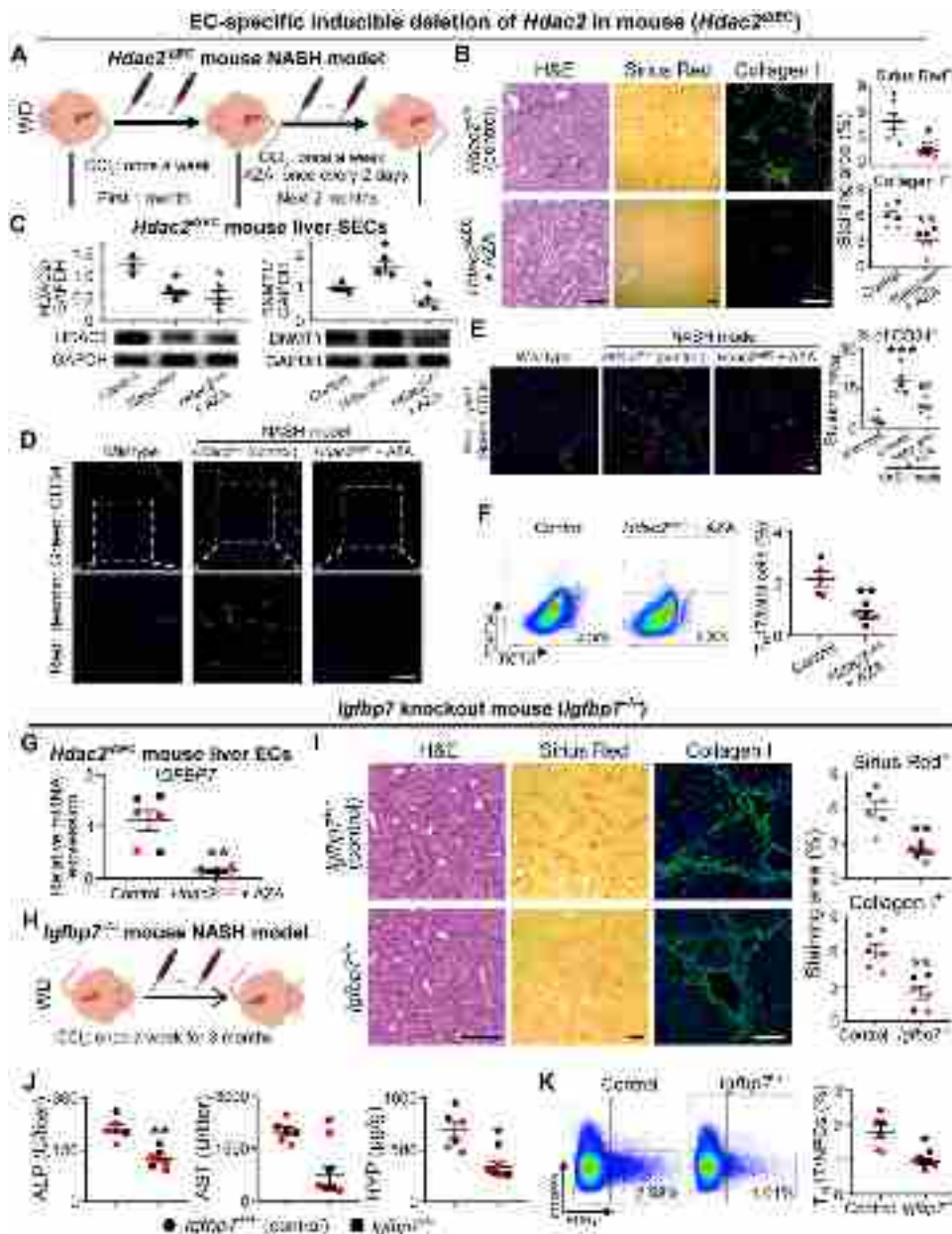


Fig. 7. Blocking HDAC2/DNMT1 and IGFBP7 in maladapted liver SECs suppresses fibrogenic TH17 cells in a mouse NASH model. (A) Schema depicting approach to test the contribution of endothelial HDAC2 in a mouse NASH model. (B) Liver histopathology analyzed by H&E, Sirius Red, and collagen I staining and quantification of control mice and mice lacking endothelial *Hdac2* (*Hdac2*^{iAEC}) treated with AZA. Scale bars, 200 μ m. *n* = 6 per group. (C) HDAC2 and DNMT1 protein abundance in liver SECs of indicated mouse groups in the NASH model as indicated by Western blots and quantification. *n* = 3 per group. (D and E) Costaining of CD34 (green) and desmin (red) (D) or Lyve1 (red) and CD34 (green) (E) in liver sections of indicated mouse groups. Scale bars, 20 μ m. *n* = 5 per group for (D) and (E). (F) Representative fluorescence-activated cell sorting (FACS) dot plots gated on CD4⁺ T cells with percentages of TH17 cells shown on the right. *n* = 5 per group. (G) *IGFBP7* expression in mouse liver ECs in the NASH model. *n* = 6 per group. (H to K) Effect of genetic knockout of *Igfbp7* on profibrotic TH17 response in the mouse NASH model. *Igfbp7*^{-/-} mice were studied in a NASH model induced by WD and CCl₄ injury (H). Liver histopathology of control and *Igfbp7*^{-/-} mice. Quantification of Sirius Red and collagen I staining shown on the right (I). Concentrations of serum ALP and AST, liver hydroxyproline amounts (J), and representative FACS dot plots showing the percentage of TH17⁺ cell in the liver (K) in control versus *Igfbp7*^{-/-} mice. *n* = 6 per group. Unpaired two-tailed Student's *t* test was applied in collagen I experiments in (B), (I), and (F), and ALP experiment in (J). Unpaired two-tailed Student's *t* test with Welch's correction was used in Sirius Red experiments in (B), (I), (G), and (K); Mann-Whitney nonparametric test without Shapiro-Wilk normality test was used in AST and Hyp experiments in (J); and one-way ANOVA followed by Tukey's post hoc test was used in (C) and (E). Data are shown as means \pm SEM. *, *Hdac2*^{iAEC}, *Hdac2*^{iAEC} + AZA, or *Igfbp7*^{-/-} versus control, or NASH model versus wild type; #, *Hdac2*^{iAEC} + AZA versus NASH model (control). **P* < 0.05; ***P* < 0.01; ****P* < 0.001. ##*P* < 0.01. Red, female; black, male.

HDAC2 and DNMT1 decreased CD34 expression in the treated group (Fig. 7, D and E). This staining result suggests a sinusoidal-to-macro liver vascular maladaptation in this mouse NASH model. Targeting endothelial HDAC2 and DNMT1 reduced TH17 cell numbers in treated mouse livers (Fig. 7F). Therefore, epigenetically maladapted liver ECs might activate a profibrotic TH17 response in a mouse NASH model.

IGFBP7 enhances the profibrotic TH17 response in a mouse NASH model

qPCR showed that combinatorial targeting of endothelial HDAC2 and DNMT1 reduced *IGFBP7* expression in the ECs of fibrotic mouse liver (Fig. 7G). To establish the functional role of *IGFBP7* in stimulating TH17 response in liver fibrosis, we analyzed the phenotype of *IGFBP7* knockout (*Igfbp7*^{-/-}) mice in a NASH model (Fig. 7H). Genetic knockout of *Igfbp7* in mice mitigated liver fibrotic responses, including collagen deposition (Fig. 7I); elevated serum AST and alkaline phosphatase (ALP) concentrations and hydroxyproline abundance (Fig. 7J); and enhanced TH17 response (Fig. 7K). To further investigate whether *IGFBP7* directly affected TH17 biology, C57BL/6J mice were intravenously injected with recombinant mouse *IGFBP7* protein (fig. S11B). Recombinant *IGFBP7* caused a greater extent of profibrotic TH17 response in injured liver than vehicle (fig. S11C). These results suggest *IGFBP7* as a mediator enhancing TH17 response that contributes to liver fibrosis.

Genetic inactivation of ADAMTS1 mitigates the profibrotic TH17 response in a mouse fibrosis model

Similar to *IGFBP7* expression, we found that *ADAMTS1* expression was attenuated in the SECs of *Hdac2*^{iAEC} + AZA mice (Fig. 8A). In addition, genetic knockdown of *ADAMTS1* in human ECs by *ADAMTS1* shRNA (sh*ADAMTS1*) blocked Smad2 phosphorylation in the presence of TGF- β 1 (Fig. 8B). Thus, we used a “human to mouse” EV transplantation approach (Fig. 8C) to investigate whether endothelial *ADAMTS1* modulates TH17 biology. EVs were collected from the cultured media from sh*ADAMTS1*- and control (shNC)-infected HUVECs. Purified endothelial EVs were intravenously

Downloaded from https://www.science.org at Sichuan University on October 06, 2021

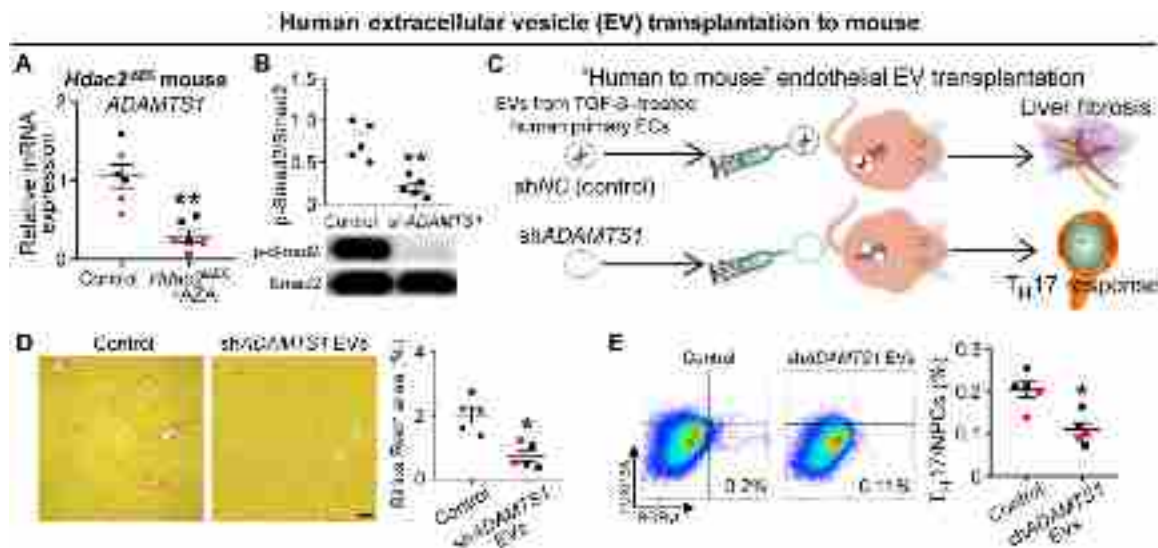


Fig. 8. ADAMTS1 suppression mitigates fibrogenic T_H17 cells in mouse fibrotic livers. (A) ADAMTS1 expression in the liver SECs of *Hdac2*^{ΔEC} mice in a NASH model. $n = 6$ per group. (B) Smad2 phosphorylation (p-Smad2) in HUVECs transduced with shADAMTS1 or control shNC. $n = 5$ per group. (C) Schema depicting approach of human to mouse EV transplantation. (D) Sirius Red staining in mice after CCl₄ injection and transplantation of shADAMTS1 or shNC EVs. Scale bar, 100 μ m. $n = 5$ per group. (E) Flow cytometry analysis of T_H17 cells in NPCs of indicated mouse groups. Percentages of T_H17 cells are shown on right. $n = 5$ per group. For all statistical analyses, data were analyzed by unpaired two-tailed Student's *t* test with Shapiro-Wilk normality test and shown as means \pm SEM. *, *Hdac2*^{ΔEC} + AZA or shADAMTS1 versus control. * $P < 0.05$; ** $P < 0.01$. Red, female; black, male.

transplanted to mice. Liver fibrosis and the T_H17 response were decreased in mice transplanted with endothelial EVs lacking ADAMTS1 compared with mice treated with control EVs (Fig. 8, D and E). These results imply the functional role of ADAMTS1 in promoting T_H17 response in liver fibrogenesis.

Our data revealed an endothelial HDAC2/DNMT1–IGFBP7/ADAMTS1– T_H17 axis contributing to liver fibrosis in human patients and minipig and mouse models of NASH. Aberrant epigenetic cross-talk in a subset of liver ECs causes vascular maladaptation that is characterized by disruption of endothelial taxonomy and generation of maladapted SECs producing profibrotic IGFBP7/ADAMTS1 in EVs (fig. S12).

DISCUSSION

NASH pathogenesis involves systemic influences including metabolic dysfunction. Endothelial and hematopoietic cells in the circulatory system are in direct contact with systemic stimuli, and NASH shares many risk factors with vascular complications (1). Therefore, we first analyzed phenotypic and molecular signatures of endothelial and hematopoietic cells in the NPCs of human patients at the single-cell level. Among the tested NPCs, vascular ECs exhibited the highest extent of change in epigenetics-related genes. This finding suggests that ECs might be more susceptible to epigenetic alterations in chronic diseases such as NASH. It is possible that ECs have a longer in vivo half-life in the circulation to accumulate more microenvironmental or systemic stimuli such as metabolic stress. As a result, scRNA-seq revealed that endothelial-selective epigenetic changes led to distortion of vascular taxonomy and profibrotic subversion of endothelial niche function in NASH. Via multiomics and multispecies analyses, we uncovered a profibrotic HDAC2/DNMT1–IGFBP7/ADAMTS1 axis in the maladapted liver EC subset. Liver fibrosis causes capillarization in SECs and alters blood

flow in the hepatic sinusoids (15, 16, 42). Liver ECs are a main component of NPCs and have been reported to constitute around 5 to 15% of NPCs. Depending on individual differences and specific isolation methods, the ratio of ECs in purified NPCs seems to vary among different studies and individuals (37, 66). In this study, scRNA-seq analysis of liver ECs suggests that chronic/metabolic injury to ECs and resulting epigenetic modification reciprocally contributes to liver fibrosis in NASH. It is likely that modification of histone and DNA in the heterogeneous hepatic vasculature stimulates maladaptation of liver ECs, and these maladapted EC subpopulations further interact with other hematopoietic cells such as T_H17 cells to jointly form fibrogenic ecosystem in NASH.

scRNA-seq allowed us to reveal the vascular maladaptation in cirrhotic liver at the single-cell level. Analysis of both human patients and a minipig NASH model shows that aberrant epigenetic cross-talk leads to a maladaptation of intraorgan endothelial taxonomy. In the tested liver samples, the observed vascular maladaptation seems to be mostly characterized with a phenotypic and functional transition within the EC lineage. Therapeutically, targeting the aberrant HDAC2/DNMT1 cross-talk normalized endothelial taxonomy to preserve parenchymal function (normal AST and ALT plasma concentrations), suggesting that endothelial maladaptation might precede hepatic damage. Functional repair of an organ requires formation of vasculature that can not only provide blood supply but also produce paracrine factors promoting regeneration and maintaining homeostasis. By contrast, maladaptation of liver ECs leads to production of fibrogenic angiocrine factors. Our findings show that epigenetics-dependent maladaptation of hepatic ECs in NASH induces profibrotic IGFBP7 and ADAMTS1 in EVs. Furthermore, in human patients and the minipig NASH model, increases in plasma IGFBP7 and ADAMTS1 preceded detectable parenchymal injury (increase in plasma AST and ALT). These clinical findings in human patients are consistent with the data showing that

targeting HDAC2/DNMT1 in ECs normalized plasma AST and ALT in the minipig NASH model. Therefore, our study implies that chronic stress in NASH stimulates epigenetic change and production of IGFBP7 and ADAMTS1, enhancing liver fibrosis. Future work will determine whether IGFBP7 or ADAMTS1 might be potential therapeutic targets or used to evaluate fibrosis progression in patients with NASH, especially in discriminating NASH from simple steatosis.

Aberrant cellular cross-talk contributes to liver fibrogenesis in NASH (2, 14). Here, we unravel the single-cell landscape of vascular adaptome. In this adaptome, epigenetically reprogrammed liver SECs produce EV IGFBP7 or ADAMTS1 to recruit profibrotic T_H17 cells. Abnormal recruitment and activation of immune cells have been shown to stimulate liver fibrosis (67–69). In this study, cellular interaction prediction analysis using scRNA-seq of NPCs showed the cross-talk between T cells and reprogrammed ECs in liver fibrosis. This prediction was supported by data showing that normalizing epigenetic change in maladapted IGFBP7⁺ADAMTS1⁺ liver SECs suppressed T_H17 enrichment in both minipig and mouse NASH models. scRNA-seq, *Igfbp7* knockout mice, and EV transplantation showed that this EC–T_H17 cross-talk at least partially depends on angiocrine IGFBP7/ADAMTS1. Therefore, bioinformatics and experimental approaches were integrated to reveal this unique profibrotic EC–T_H17 cell interaction. Given the systemic distribution of vascular and hematopoietic cells in multiple organs, decoding the vascular adaptation node molecule might help identify therapeutic targets or biomarkers for fibrotic diseases in other organs.

Building on the findings from human patients, we used complementary preclinical NASH models (minipig and mouse) to define the contribution of epigenetics-dependent vascular maladaptation. The digestive system of the minipig exhibits close analogy to that of humans (70). Therefore, the minipig offers the advantage of resembling human metabolic disorder-related diseases such as NASH. The minipig model also enables liver biopsy for multiomics assessment of therapeutic effects and underlying mechanisms. Compared with the minipig, genetically modified mice such as EC-specific *Hdac2* knockout and *Igfbp7* knockout mice provide tools for defining the cellular and molecular mechanisms involved in epigenetics-dependent vascular maladaptation. Pharmacological and genetic targeting experiments in the minipig and mouse NASH models revealed that abnormal HDAC2/DNMT1 cross-talk causes vascular maladaptation and subsequent production of IGFBP7/ADAMTS1 in ECs. These data are in line with the identified correlation between HDAC2, DNMT1, IGFBP7, or ADAMTS1 induction and fibrosis progression in human cirrhotic patients. In both mouse and minipig NASH models, combinatorial targeting of HDAC2 and DNMT1 showed synergistic antifibrotic effects. Administration of IGFBP7- and ADAMTS1-containing endothelial EV further suggests the fibrogenic role of ADAMTS1/IGFBP7 via stimulating T_H17 response in the liver. Therefore, our preclinical platforms might aid in devising therapy for fibrosis-related diseases, which are associated with 40% of deaths worldwide (71).

This study has some limitations because of technical hurdles. We assessed liver cell propagation in the minipig NASH model using Ki67 staining. Immunohistochemical staining of Ki67 showed that HDAC2i and DNMT1i treatment enhanced the mitosis in liver cells exhibiting hepatocyte features such as distinctly round nuclei and polygonal shape. However, we were not fully able to illustrate the

specific cell proliferation of hepatocytes with costaining because of the lack of an antibody faithfully recognizing minipig hepatocytes. In addition, liver SECs undergoing capillarization start to express CD34 that is normally expressed by MECs. Therefore, we mainly purified noncapillarized SECs in the fibrotic liver with our current isolation approach, and the results obtained mostly reflect the phenotype of the CD45⁺CD34⁺CD31⁺ SEC subpopulation during liver fibrogenesis. In the future, these hurdles might be overcome with better antibodies for detection and isolation of different types of ECs or hepatocytes in multiple species. Furthermore, because of the experimental cost, we tested male minipigs in the NASH model. To illustrate the possible influence of gender on the outcome, we presented male and female patient and mouse data with different colors in the graphs.

In this study, we uncovered a single-cell landscape of vascular adaptation in which epigenetically reprogrammed EC subset stimulates T_H17 cells to jointly contribute to liver fibrosis in multiple species. Formation of this maladaptive vascular adaptome involves distortion of endothelial taxonomy and production of fibrogenic factors in EVs. Elucidating the molecular and cellular network underlying this vascular adaptation might help to discover diagnostic or therapeutic candidates for fibrotic diseases.

MATERIALS AND METHODS

Study design

This study aimed to evaluate how maladaptation of vascular niche provokes liver fibrosis in NASH. We used multiomics approaches to reveal the landscape of vascular adaptation in which ECs, paracrine/angiocrine factors, circulating EVs, and T_H17 cells jointly contribute to liver fibrosis and cirrhosis in human, minipig, and mouse. To establish the clinical value of effector molecules IGFBP7 and ADAMTS1, we used a human plasma cohort that included healthy volunteers, simple steatosis, early-stage NASH (F0 to F1), and fibrotic/cirrhotic patients (without cancer) to assess the concentrations of IGFBP7 and ADAMTS1 in human patient plasma. We used a human to mouse EV transplantation approach and genetic mouse models to illustrate the functional contribution of angiocrine IGFBP7 and ADAMTS1 to liver fibrosis. Three to five (human), three (minipig), and five to six (mouse) biological samples were used for each experiment. We did not differentiate between genders in human or mouse samples. All studies were approved by the Ethics Committees of West China Second University Hospital, West China Hospital of Sichuan University, and Chengdu Dossy Biological Technology Co. Ltd.

Patients and clinical specimens

Patient liver and plasma samples were collected with informed consent at West China Hospital, Sichuan University at Chengdu, China. The healthy liver tissues (without fibrosis) were obtained from patients with hepatic hemangiomas who underwent endoscopic hepatectomy. The cirrhotic liver tissues were obtained from patients with histologically diagnosed liver fibrosis. Patient information for scRNA-seq, liquid chip analysis, and gene expression analysis is shown in table S1. Plasma samples were obtained from healthy volunteers ($n = 21$), patients with simple steatosis ($n = 16$), patients with early-stage NASH (F0 to F1) ($n = 12$), and fibrotic/cirrhotic/NASH patients (without cancer) ($n = 75$) of different pathological grades. We used fibrosis-4 score (Fib-4) and transient

elastography (TE) to determine the grade of fibrosis in non-NASH livers and used NAFLD fibrosis score, Fib-4, TE, and controlled attenuation parameter to determine the grade of fibrosis and steatosis in NASH livers (72, 73). Early-stage NASH was mainly identified by the histology of liver biopsy samples; some other samples were also identified by the histology of liver biopsy. Patient information for plasma analysis is shown in data file S1. The Medical Ethics Committee of West China Hospital of Sichuan University approved the study. The study on human subjects conformed to the principles of the Declaration of Helsinki.

Minipigs

Bama minipigs were obtained from Chengdu Dossy Biological Technology Co. Ltd., China. The study was performed in male minipigs. Minipigs were kept in independent cages at Chengdu Dossy Experimental Animals Center, fed with diet containing 2% cholesterol and 30% fat by weight, and supplemented with fructose and glucose. The Laboratory Animal Ethics Committee of West China Second University Hospital, Sichuan University, and Chengdu Dossy Biological Technology Co. Ltd. approved the minipig experiments.

Mice

C57BL/6J mice were obtained from the Model Animal Research Center of Nanjing University. C57BL/6J-*Hdac2*^{em1(flox)Smoc} mice were obtained from Shanghai Model Organisms Center Inc. *Igfbp7*^{-/-} mice were from GemPharmatech, Nanjing, China. Mice expressing EC-specific *Cdh5*-(PAC)-Cre^{ERT2} were provided by R. H. Adam (74). *Cdh5*-(PAC)-Cre^{ERT2} mouse was crossed with floxed *Hdac2* mouse to generate *Hdac2*^{ΔEC/ΔEC} (*Hdac2*^{ΔEC}). *Hdac2*^{ΔEC} mice were intraperitoneally treated with tamoxifen (250 mg/kg) 2 months after birth for 6 days (interrupted for 3 days after the third dose), leading to endothelial-specific deletion of *Hdac2*. Mice were kept in the pathogen-free facility at the Experimental Center of West China Second University Hospital and fed ad libitum on a standard 12-hour light/dark cycle. The protocols of the animal experiments were approved by the Laboratory Animal Ethics Committee of West China Second University Hospital, Sichuan University.

Statistical analysis

All calculations or analyses were performed using Prism 8 software package (GraphPad) or R. Data were statistically analyzed by unpaired two-tailed Student's *t* test with Shapiro-Wilk normality test or Mann-Whitney nonparametric test without Shapiro-Wilk normality test (two-group comparisons) and one-way analysis of variance (ANOVA) followed by Tukey's post hoc test (more than two-group comparisons). Differential expression genes between two groups of cells were identified using a Wilcoxon rank sum test in scRNA-seq. All data are presented as means ± SEM. *P* < 0.05 was considered statistically significant, and all error bars represent SEM. For in vivo experiments, *n* indicates the data from individual biological replicate. All statistical tests, sample sizes, and comparisons are included in the figures and figure legends. In all cases, * indicates a statistical difference between cirrhotic, fibrotic, or NASH versus healthy/control group; # indicates a statistical difference between treated versus cirrhotic, fibrotic, or NASH group, or NASH versus simple steatosis group. **P* < 0.05 or #*P* < 0.05; ***P* < 0.01 or ##*P* < 0.01; ****P* < 0.001; *****P* < 0.0001. Additional materials and methods are given in the Supplementary Materials.

SUPPLEMENTARY MATERIALS

www.science.org/doi/10.1126/scitranslmed.abd1206

Supplementary Materials and Methods

Figs. S1 to S12

Tables S1 to S3

Data files S1 and S2

References (75–77)

[View/request a protocol for this paper from Bio-protocol.](#)

REFERENCES AND NOTES

1. S. L. Friedman, B. A. Neuschwander-Tetri, M. Rinella, A. J. Sanyal, Mechanisms of NAFLD development and therapeutic strategies. *Nat. Med.* **24**, 908–922 (2018).
2. R. F. Schwabe, I. Tabas, U. B. Pajvani, Mechanisms of fibrosis development in nonalcoholic steatohepatitis. *Gastroenterology* **158**, 1913–1928 (2020).
3. X. Wang, Z. Zheng, J. M. Caviglia, K. E. Corey, T. M. Herfel, B. Cai, R. Masia, R. T. Chung, J. H. Lefkowitz, R. F. Schwabe, I. Tabas, Hepatocyte TAZ/WWTR1 promotes inflammation and fibrosis in nonalcoholic steatohepatitis. *Cell Metab.* **24**, 848–862 (2016).
4. R. Bataller, D. A. Brenner, Liver fibrosis. *J. Clin. Invest.* **115**, 209–218 (2005).
5. S. K. Asrani, H. Devarbahi, J. Eaton, P. S. Kamath, Burden of liver diseases in the world. *J. Hepatol.* **70**, 151–171 (2019).
6. S. Sookoian, C. J. Pirola, Repurposing drugs to target nonalcoholic steatohepatitis. *World J. Gastroenterol.* **25**, 1783–1796 (2019).
7. Z. M. Younossi, A. B. Koenig, D. Abdelatif, Y. Fazel, L. Henry, M. Wymer, Global epidemiology of nonalcoholic fatty liver disease—Meta-analytic assessment of prevalence, incidence, and outcomes. *Hepatology* **64**, 73–84 (2016).
8. R. Weiskirchen, F. Tacke, Relevance of autophagy in parenchymal and non-parenchymal liver cells for health and disease. *Cells* **8**, 16 (2019).
9. S. A. MacParland, J. C. Liu, X.-Z. Ma, B. T. Innes, A. M. Bartczak, B. K. Gage, J. Manuel, N. Khuu, J. Echeverri, I. Linares, R. Gupta, M. L. Cheng, L. Y. Liu, D. Camat, S. W. Chung, R. K. Seliga, Z. Shao, E. Lee, S. Ogawa, M. Ogawa, M. D. Wilson, J. E. Fish, M. Selzner, A. Ghanekar, D. Grant, P. Greig, G. Sapisochin, N. Selzner, N. Winegarden, O. Adeyi, G. Keller, G. D. Bader, I. D. McGilvray, Single cell RNA sequencing of human liver reveals distinct intrahepatic macrophage populations. *Nat. Commun.* **9**, 4383 (2018).
10. V. Krizhanovsky, M. Yon, R. A. Dickins, S. Hearn, J. Simon, C. Miething, H. Yee, L. Zender, S. W. Lowe, Senescence of activated stellate cells limits liver fibrosis. *Cell* **134**, 657–667 (2008).
11. B. Cai, P. Dongiovanni, K. E. Corey, X. Wang, I. O. Shmarakov, Z. Zheng, C. Kasikara, V. Davra, M. Meroni, R. T. Chung, C. V. Rothlin, R. F. Schwabe, W. S. Blaner, R. B. Birge, L. Valenti, I. Tabas, Macrophage MerTK promotes liver fibrosis in nonalcoholic steatohepatitis. *Cell Metab.* **31**, 406–421.e7 (2020).
12. C. Yin, K. J. Evason, K. Asahina, D. Y. R. Stainier, Hepatic stellate cells in liver development, regeneration, and cancer. *J. Clin. Invest.* **123**, 1902–1910 (2013).
13. S. L. Friedman, D. Sheppard, J. S. Duffield, S. Violette, Therapy for fibrotic diseases: Nearing the starting line. *Sci. Transl. Med.* **5**, 167s1 (2013).
14. G. Marrone, V. H. Shah, J. Gracia-Sancho, Sinusoidal communication in liver fibrosis and regeneration. *J. Hepatol.* **65**, 608–617 (2016).
15. L. Wang, X. Wang, G. Xie, L. Wang, C. K. Hill, L. D. Deleve, Liver sinusoidal endothelial cell progenitor cells promote liver regeneration in rats. *J. Clin. Invest.* **122**, 1567–1573 (2012).
16. J. S. Lee, D. Semela, J. Iredale, V. H. Shah, Sinusoidal remodeling and angiogenesis: A new function for the liver-specific pericyte? *Hepatology* **45**, 817–825 (2007).
17. K. Mukai, M. Tsai, H. Saito, S. J. Galli, Mast cells as sources of cytokines, chemokines, and growth factors. *Immunol. Rev.* **282**, 121–150 (2018).
18. K. Wilhelm, K. Happel, G. Eelen, S. Schoors, M. F. Oellerich, R. Lim, B. Zimmermann, I. M. Aspalter, C. A. Franco, T. Boettger, T. Braun, M. Fruttiger, K. Rajewsky, C. Keller, J. C. Bruning, H. Gerhardt, P. Carmeliet, M. Potente, FOXO1 couples metabolic activity and growth state in the vascular endothelium. *Nature* **529**, 216–220 (2016).
19. P. Yu, K. Wilhelm, A. Dubrac, J. K. Tung, T. C. Alves, J. S. Fang, Y. Xie, J. Zhu, Z. Chen, F. De Smet, J. Zhang, S. W. Jin, L. Sun, H. Sun, R. G. Kibbey, K. K. Hirschi, N. Hay, P. Carmeliet, T. W. Chittenden, A. Eichmann, M. Potente, M. Simons, FGF-dependent metabolic control of vascular development. *Nature* **545**, 224–228 (2017).
20. B. S. Ding, Z. Cao, R. Lis, D. J. Nolan, P. Guo, M. Simons, M. E. Penfold, K. Shido, S. Y. Rabbany, S. Raffii, Divergent angiocrine signals from vascular niche balance liver regeneration and fibrosis. *Nature* **505**, 97–102 (2014).
21. B. Wang, L. Zhao, M. Fish, C. Y. Logan, R. Nusse, Self-renewing diploid Axin2⁺ cells fuel homeostatic renewal of the liver. *Nature* **524**, 180–185 (2015).
22. K. Yoshioka, M. Kunitomo, K. Yanai, H. Shimizu, S. Nakasono, T. Negishi, M. Dateki, Hepatocyte nuclear factor 1β induced by chemical stress accelerates cell proliferation and increases genomic instability in mouse liver. *J. Recept. Signal Transduct. Res.* **31**, 132–138 (2011).
23. K. S. Zaret, M. Grompe, Generation and regeneration of cells of the liver and pancreas. *Science* **322**, 1490–1494 (2008).

24. S. Lin, E. M. Nascimento, C. R. Gajera, L. Chen, P. Neuhofer, A. Garbuzov, S. Wang, S. E. Artandi, Distributed hepatocytes expressing telomerase repopulate the liver in homeostasis and injury. *Nature* **556**, 244–248 (2018).
25. A. Lujambio, L. Akkari, J. Simon, D. Grace, D. F. Tschaharganeh, J. E. Bolden, Z. Zhao, V. Thapar, J. A. Joyce, V. Krizhanovskiy, S. W. Lowe, Non-cell-autonomous tumor suppression by p53. *Cell* **153**, 449–460 (2013).
26. A. W. Duncan, M. H. Taylor, R. D. Hickey, A. E. Hanlon Newell, M. L. Lenzi, S. B. Olson, M. J. Finegold, M. Grompe, The ploidy conveyor of mature hepatocytes as a source of genetic variation. *Nature* **467**, 707–710 (2010).
27. J. Kalucka, L. P. M. H. de Rooij, J. Goveia, K. Rohlenova, S. J. Dumas, E. Meta, N. V. Concinha, F. Taverna, L.-A. Teuwen, K. Veys, M. Garcia-Caballero, S. Khan, V. Geldhof, L. Sokol, R. Chen, L. Treps, M. Borri, P. de Zeeuw, C. Dubois, T. K. Karakach, K. D. Falkenberg, M. Parys, X. Yin, S. Vinckier, Y. Du, R. A. Fenton, L. Schoonjans, M. Dewerchin, G. Eelen, B. Thienpont, L. Lin, L. Bolund, X. Li, Y. Luo, P. Carmeliet, Single-cell transcriptome atlas of murine endothelial cells. *Cell* **180**, 764–779.e20 (2020).
28. H. G. Augustin, G. Y. Koh, Organotypic vasculature: From descriptive heterogeneity to functional pathophysiology. *Science* **357**, eaal2379 (2017).
29. P. Carmeliet, R. K. Jain, Molecular mechanisms and clinical applications of angiogenesis. *Nature* **473**, 298–307 (2011).
30. K. J. Png, N. Halberg, M. Yoshida, S. F. Tavazoie, A microRNA regulon that mediates endothelial recruitment and metastasis by cancer cells. *Nature* **481**, 190–194 (2011).
31. E. M. Zeisberg, O. Tarnavski, M. Zeisberg, A. L. Dorfman, J. R. McMullen, E. Gustafsson, A. Chandraker, X. Yuan, W. T. Pu, A. B. Roberts, E. G. Neilson, M. H. Sayegh, S. Izumo, R. Kalluri, Endothelial-to-mesenchymal transition contributes to cardiac fibrosis. *Nat. Med.* **13**, 952–961 (2007).
32. J. LeCouter, D. R. Moritz, B. Li, G. L. Phillips, X. H. Liang, H. P. Gerber, K. J. Hillan, N. Ferrara, Angiogenesis-independent endothelial protection of liver: Role of VEGFR-1. *Science* **299**, 890–893 (2003).
33. Y. Manavski, T. Abel, J. Hu, D. Kleinlutzum, C. J. Buchholz, C. Belz, H. G. Augustin, R. A. Boon, S. Dimmeler, Endothelial transcription factor KLF2 negatively regulates liver regeneration via induction of activin A. *Proc. Natl. Acad. Sci. U.S.A.* **114**, 3993–3998 (2017).
34. J. Hu, K. Srivastava, M. Wieland, A. Runge, C. Mogler, E. Besemfelder, D. Terhardt, M. J. Vogel, L. Cao, C. Korn, S. Bartels, M. Thomas, H. G. Augustin, Endothelial cell-derived angiopoietin-2 controls liver regeneration as a spatiotemporal rheostat. *Science* **343**, 416–419 (2014).
35. M. Nikfarjam, V. Muralidharan, C. Malcontenti-Wilson, C. Christophi, Scanning electron microscopy study of the blood supply of human colorectal liver metastases. *Eur. J. Surg. Oncol.* **29**, 856–861 (2003).
36. I. Kassisia, A. Brault, P. M. Huet, Hepatic artery and portal vein vascularization of normal and cirrhotic rat liver. *Hepatology* **19**, 1189–1197 (1994).
37. P. Ramachandran, R. Dobie, J. R. Wilson-Kanamori, E. F. Dora, B. E. P. Henderson, N. T. Luu, J. R. Portman, K. P. Matchett, M. Brice, J. A. Marwick, R. S. Taylor, M. Efreмова, R. Vento-Tormo, N. O. Carragher, T. J. Kendall, J. A. Fallowfield, E. M. Harrison, D. J. Mole, S. J. Wigmore, P. N. Newsome, C. J. Weston, J. P. Iredale, F. Tacke, J. W. Pollard, C. P. Ponting, J. C. Marioni, S. A. Teichmann, N. C. Henderson, Resolving the fibrotic niche of human liver cirrhosis at single-cell level. *Nature* **575**, 512–518 (2019).
38. N. Aizarani, A. Saviano, Sagar, L. Mailly, S. Durand, J. S. Herman, P. Pessaux, T. F. Baumert, D. Grün, A human liver cell atlas reveals heterogeneity and epithelial progenitors. *Nature* **572**, 199–204 (2019).
39. B. S. Ding, D. J. Nolan, J. M. Butler, D. James, A. O. Babazadeh, Z. Rosenwaks, V. Mittal, H. Kobayashi, K. Shido, D. Lyden, T. N. Sato, S. Y. Rabbany, S. Rafii, Inductive angiocrine signals from sinusoidal endothelium are required for liver regeneration. *Nature* **468**, 310–315 (2010).
40. S. Rafii, J. M. Butler, B. S. Ding, Angiocrine functions of organ-specific endothelial cells. *Nature* **529**, 316–325 (2016).
41. S. K. Ramasamy, A. P. Kusumbe, T. Itkin, S. Gur-Cohen, T. Lapidot, R. H. Adams, Regulation of hematopoiesis and osteogenesis by blood vessel-derived signals. *Annu. Rev. Cell Dev. Biol.* **32**, 649–675 (2016).
42. A. C. Straub, K. A. Clark, M. A. Ross, A. G. Chandra, S. Li, X. Gao, P. J. Pagano, D. B. Stolz, A. Barchowsky, Arsenic-stimulated liver sinusoidal capillarization in mice requires NADPH oxidase-generated superoxide. *J. Clin. Invest.* **118**, 3980–3989 (2008).
43. T. Su, Y. Iwakiri, Novel endothelial LECT2/Tie1 signaling in liver fibrosis. *Hepatology* **72**, 347–349 (2020).
44. K. Furrer, A. Rickenbacher, Y. Tian, W. Jochum, A. G. Bittermann, A. Kach, B. Humar, R. Graf, W. Moritz, P. A. Clavien, Serotonin reverts age-related capillarization and failure of regeneration in the liver through a VEGF-dependent pathway. *Proc. Natl. Acad. Sci. U.S.A.* **108**, 2945–2950 (2011).
45. A. L. Gomes, A. Teijeiro, S. Buren, K. S. Tummala, M. Yilmaz, A. Waisman, J. P. Theurillat, C. Perna, N. Djouder, Metabolic inflammation-associated IL-17A causes non-alcoholic steatohepatitis and hepatocellular carcinoma. *Cancer Cell* **30**, 161–175 (2016).
46. T. Hardy, D. A. Mann, Epigenetics in liver disease: From biology to therapeutics. *Gut* **65**, 1895–1905 (2016).
47. C. L. Wilson, D. A. Mann, L. A. Borthwick, Epigenetic reprogramming in liver fibrosis and cancer. *Adv. Drug Deliv. Rev.* **121**, 124–132 (2017).
48. W. Bechtel, S. McGoohan, E. M. Zeisberg, G. A. Muller, H. Kalbacher, D. J. Salant, C. A. Muller, R. Kalluri, M. Zeisberg, Methylation determines fibroblast activation and fibrogenesis in the kidney. *Nat. Med.* **16**, 544–550 (2010).
49. M. Wang, Q. Gong, J. Zhang, L. Chen, Z. Zhang, L. Lu, D. Yu, Y. Han, D. Zhang, P. Chen, X. Zhang, Z. Yuan, J. Huang, X. Zhang, Characterization of gene expression profiles in HBV-related liver fibrosis patients and identification of ITGBl1 as a key regulator of fibrogenesis. *Sci. Rep.* **7**, 43446 (2017).
50. M. J. Topper, M. Vaz, K. B. Chiappinelli, C. E. DeStefano Shields, N. Niknafs, R.-W. C. Yen, A. Wenzel, J. Hicks, M. Ballew, M. Stone, P. T. Tran, C. A. Zahnow, M. D. Hellmann, V. Anagnostou, P. L. Strissel, R. Strick, V. E. Velculescu, S. B. Baylin, Epigenetic therapy ties MYC depletion to reversing immune evasion and treating lung cancer. *Cell* **171**, 1284–1300.e21 (2017).
51. T. Tsuchida, Y. A. Lee, N. Fujiwara, M. Ybanez, B. Allen, S. Martins, M. I. Fiel, N. Goossens, H. I. Chou, Y. Hoshida, S. L. Friedman, A simple diet- and chemical-induced murine NASH model with rapid progression of steatohepatitis, fibrosis and liver cancer. *J. Hepatol.* **69**, 385–395 (2018).
52. L. Lorenz, J. Axnick, T. Buschmann, C. Henning, S. Urner, S. Fang, H. Nurmi, N. Eichhorst, R. Holtmeier, K. Bodis, J. H. Hwang, K. Mussig, D. Eberhard, J. Stypmann, O. Kuss, M. Roden, K. Alitalo, D. Haussinger, E. Lammert, Mechanosensing by $\beta 1$ integrin induces angiocrine signals for liver growth and survival. *Nature* **562**, 128–132 (2018).
53. J. D. Buenrostro, P. G. Giresi, L. C. Zaba, H. Y. Chang, W. J. Greenleaf, Transposition of native chromatin for fast and sensitive epigenomic profiling of open chromatin, DNA-binding proteins and nucleosome position. *Nat. Methods* **10**, 1213–1218 (2013).
54. M. Xu, H.-H. Xu, Y. Lin, X. Sun, L.-J. Wang, Z.-P. Fang, X.-H. Su, X.-J. Liang, Y. Hu, Z.-M. Liu, Y. Cheng, Y. Wei, J. Li, L. Li, H.-J. Liu, Z. Cheng, N. Tang, C. Peng, T. Li, T. Liu, L. Qiao, D. Wu, Y. Q. Ding, W.-J. Zhou, LECT2, a ligand for Tie1, plays a crucial role in liver fibrogenesis. *Cell* **178**, 1478–1492.e20 (2019).
55. R. Kalluri, V. S. LeBleu, The biology, function, and biomedical applications of exosomes. *Science* **367**, eaau6977 (2020).
56. A. Becker, B. K. Thakur, J. M. Weiss, H. S. Kim, H. Peinado, D. Lyden, Extracellular vesicles in cancer: Cell-to-cell mediators of metastasis. *Cancer Cell* **30**, 836–848 (2016).
57. C. Théry, S. Amigorena, G. Raposo, A. Clayton, Isolation and characterization of exosomes from cell culture supernatants and biological fluids. *Curr. Protoc. Cell Biol.* **Chapter 3**, Unit 3.22 (2006).
58. R. Vento-Tormo, M. Efreмова, R. A. Botting, M. Y. Turco, M. Vento-Tormo, K. B. Meyer, J.-E. Park, E. Stephenson, K. Polanski, A. Goncalves, L. Gardner, S. Holmqvist, J. Henriksson, A. Zou, A. M. Sharkey, B. Millar, B. Innes, L. Wood, A. Wilbrey-Clark, R. P. Payne, M. A. Ivarsson, S. Lisgo, A. Filby, D. H. Rowitch, J. N. Bulmer, G. J. Wright, M. J. T. Stubbington, M. Haniffa, A. Moffett, S. A. Teichmann, Single-cell reconstruction of the early maternal-fetal interface in humans. *Nature* **563**, 347–353 (2018).
59. E. Komiya, M. Furuya, N. Watanabe, Y. Miyagi, S. Higashi, K. Miyazaki, Elevated expression of angiomodulin (AGM/IGFBP-rP1) in tumor stroma and its roles in fibroblast activation. *Cancer Sci.* **103**, 691–699 (2012).
60. K. Bourd-Boittin, D. Bonnier, A. Leyme, B. Mari, P. Tuffery, M. Samson, F. Ezan, G. Baffet, N. Theret, Protease profiling of liver fibrosis reveals the ADAM metalloproteinase with thrombospondin type 1 motif, 1 as a central activator of transforming growth factor beta. *Hepatology* **54**, 2173–2184 (2011).
61. P. R. Mangan, L. E. Harrington, D. B. O’Quinn, W. S. Helms, D. C. Bullard, C. O. Elson, R. D. Hatton, S. M. Wahl, T. R. Schoeb, C. T. Weaver, Transforming growth factor- β induces development of the Th17 lineage. *Nature* **441**, 231–234 (2006).
62. C. M. Chackelevicius, S. E. Gambaro, C. Tiribelli, N. Rosso, Th17 involvement in nonalcoholic fatty liver disease progression to non-alcoholic steatohepatitis. *World J. Gastroenterol.* **22**, 9096–9103 (2016).
63. J. Zhao, Z. Zhang, Y. Luan, Z. Zou, Y. Sun, Y. Li, L. Jin, C. Zhou, J. Fu, B. Gao, Y. Fu, F. S. Wang, Pathological functions of interleukin-22 in chronic liver inflammation and fibrosis with hepatitis B virus infection by promoting T helper 17 cell recruitment. *Hepatology* **59**, 1331–1342 (2014).
64. N. Malhotra, E. Robertson, J. Kang, SMAD2 is essential for TGF β -mediated Th17 cell generation. *J. Biol. Chem.* **285**, 29044–29048 (2010).
65. H. Urushima, M. Fujimoto, T. Mishima, T. Ohkawara, H. Honda, H. Lee, H. Kawahata, S. Serada, T. Naka, Leucine-rich alpha 2 glycoprotein promotes Th17 differentiation and collagen-induced arthritis in mice through enhancement of TGF- β -Smad2 signaling in naïve helper T cells. *Arthritis Res. Ther.* **19**, 137 (2017).
66. E. Pfeiffer, V. Kegel, K. Zeilinger, J. G. Hengstler, A. K. Nüssler, D. Seehofer, G. Damm, Featured article: Isolation, characterization, and cultivation of human hepatocytes and non-parenchymal liver cells. *Exp. Biol. Med. (Maywood)* **240**, 645–656 (2015).

67. R. L. Gieseck III, M. S. Wilson, T. A. Wynn, Type 2 immunity in tissue repair and fibrosis. *Nat. Rev. Immunol.* **18**, 62–76 (2018).
68. S. J. Galli, N. Borregaard, T. A. Wynn, Phenotypic and functional plasticity of cells of innate immunity: Macrophages, mast cells and neutrophils. *Nat. Immunol.* **12**, 1035–1044 (2011).
69. T. A. Wynn, A. Chawla, J. W. Pollard, Macrophage biology in development, homeostasis and disease. *Nature* **496**, 445–455 (2013).
70. L. Lee, M. Alloosh, R. Saxena, W. Van Alstine, B. A. Watkins, J. E. Klaunig, M. Sturek, N. Chalasani, Nutritional model of steatohepatitis and metabolic syndrome in the Ossabaw miniature swine. *Hepatology* **50**, 56–67 (2009).
71. D. C. Rockey, P. D. Bell, J. A. Hill, Fibrosis — A common pathway to organ injury and failure. *N. Engl. J. Med.* **372**, 1138–1149 (2015).
72. L. Castera, M. Friedrich-Rust, R. Loomba, Noninvasive assessment of liver disease in patients with nonalcoholic fatty liver disease. *Gastroenterology* **156**, 1264–1281.e4 (2019).
73. Z. M. Younossi, M. Noureddin, D. Bernstein, P. Kwo, M. Russo, M. L. Shiffman, Z. Younes, M. Abdelmalek, Role of noninvasive tests in clinical gastroenterology practices to identify patients with nonalcoholic steatohepatitis at high risk of adverse outcomes: Expert panel recommendations. *Am. J. Gastroenterol.* **116**, 254–262 (2021).
74. Y. Wang, M. Nakayama, M. E. Pitulescu, T. S. Schmidt, M. L. Bochenek, A. Sakakibara, S. Adams, A. Davy, U. Deutsch, U. Luthi, A. Barberis, L. E. Benjamin, T. Makinen, C. D. Nobes, R. H. Adams, Ephrin-B2 controls VEGF-induced angiogenesis and lymphangiogenesis. *Nature* **465**, 483–486 (2010).
75. H. Zhang, Y. Liu, L. Wang, Z. Li, H. Zhang, J. Wu, N. Rahman, Y. Guo, D. Li, N. Li, I. Huhtaniemi, S. Y. Tsang, G. F. Gao, X. Li, Differential effects of estrogen/androgen on the prevention of nonalcoholic fatty liver disease in the male rat. *J. Lipid Res.* **54**, 345–357 (2013).
76. R. Satija, J. A. Farrell, D. Gennert, A. F. Schier, A. Regev, Spatial reconstruction of single-cell gene expression data. *Nat. Biotechnol.* **33**, 495–502 (2015).
77. A. Butler, P. Hoffman, P. Smibert, E. Papalexji, R. Satija, Integrating single-cell transcriptomic data across different conditions, technologies, and species. *Nat. Biotechnol.* **36**, 411–420 (2018).

Funding: This work was supported by the Key Research and Development Program focused on Stem Cell and Translational Research (2016YFA0101600), National Science Foundation of China (91639117, 81941007, 81925005, 81722005, 91839301, 81600771, and 81900512), Sichuan Science and Technology Program (2019JDJQ0030, 2019YJ0059), and China Postdoctoral Science Foundation (2018M643489). S.L.F. is supported by the National Institute of Diabetes and Digestive and Kidney Diseases (RO1DK56621 and RO1DK128289). **Author contributions:** H.Z., Y.M., X.C., D.W., and X.H. designed and performed the experiments, analyzed the data, and wrote the manuscript. B.C., Y.R., W.J., X.T., T.B., Y.C., Y.Z., C.Z., X.X., J.L., and Y.D. performed the experiments. T.Y., Lu Chen, and H.-M.L. provided suggestions on the project design. S.L.F. commented on the results and revised the manuscript. Liping Chen supervised human data and revised the manuscript. Z.C. and B.-S.D. conceived the project, designed and supervised the experiments, and wrote and revised the manuscript. **Competing interests:** The authors declare that they have no competing interests. **Data and materials availability:** scRNA-seq data that support the findings of this study have been deposited in NCBI Gene Expression Omnibus (accession GSE181483). Patient data are available in data file S1 and raw data in data file S2. All data associated with this study are present in the paper or the Supplementary Materials.

Submitted 2 June 2020

Resubmitted 2 February 2021

Accepted 6 August 2021

Published 6 October 2021

10.1126/scitranslmed.abd1206

Citation: H. Zhang, Y. Ma, X. Cheng, D. Wu, X. Huang, B. Chen, Y. Ren, W. Jiang, X. Tang, T. Bai, Y. Chen, Y. Zhao, C. Zhang, X. Xiao, J. Liu, Y. Deng, T. Ye, L. Chen, H.-M. Liu, S. L. Friedman, L. Chen, B.-S. Ding, Z. Cao, Targeting epigenetically maladapted vascular niche alleviates liver fibrosis in nonalcoholic steatohepatitis. *Sci. Transl. Med.* **13**, eabd1206 (2021).

Targeting epigenetically maladapted vascular niche alleviates liver fibrosis in nonalcoholic steatohepatitis

Hua Zhang Yongyuan Ma Xinying Cheng Dongbo Wu Xingming Huang Bin Chen Yafeng Ren Wei Jiang Xiaoqiang Tang Ting Bai Yutian Chen Yilin Zhao Chunxue Zhang Xia Xiao Jing Liu Yue Deng Tinghong Ye Lu Chen Han-Min Liu Scott L. Friedman Liping Chen Bi-Sen Ding Zhongwei Cao

Sci. Transl. Med., 13 (614), eabd1206.

Epigenetic bad actors in liver fibrosis

The molecular processes that lead to fibrogenesis in nonalcoholic steatohepatitis (NASH) are complex and not completely understood. Zhang *et al.* used single-cell omics analysis of multiple species to show that epigenetic dysregulation of hepatic endothelial cells promoted the maladaptation of these cells from a sinusoidal to vascular phenotype. The vascularly maladapted cells stimulated fibrosis via a HDAC2-DNMT1-IGFBP7-T17 pathway, and HDAC2 and DNMT1 inhibitors targeting this pathway mitigated fibrosis in a minipig NASH model. This provides a valuable resource for studying NASH pathogenesis and suggests a potential strategy to block the liver fibrosis promoted by maladaptive vascularization in this disease.

View the article online

<https://www.science.org/doi/10.1126/scitranslmed.abd1206>

Permissions

<https://www.science.org/help/reprints-and-permissions>

Use of think article is subject to the [Terms of service](#)